Monthly Notices
of the
ROYAL ASTRONOMICAL SOCIETY

MNRAS **438,** 368–387 (2014)
Advance Access publication 2013 December 13

doi:10.1093/mnras/stt2203

SN 2009N: linking normal and subluminous Type II-P SNe

K. Takáts,[1,2⋆] M. L. Pumo,[3,4] N. Elias-Rosa,[3,5] A. Pastorello,[3] G. Pignata,[1] E. Paillas,[1] L. Zampieri,[3] J. P. Anderson,[6] J. Vinkó,[2] S. Benetti,[3] M.-T. Botticella,[7,8] F. Bufano,[1,3] A. Campillay,[9] R. Cartier,[6] M. Ergon,[10] G. Folatelli,[11] R. J. Foley,[12,13] F. Förster,[6] M. Hamuy,[6] V.-P. Hentunen,[14] E. Kankare,[15] G. Leloudas,[16,17] N. Morrell,[9] M. Nissinen,[14] M. M. Phillips,[9] S. J. Smartt,[8] M. Stritzinger,[18] S. Taubenberger,[19] S. Valenti,[20,21] S. D. Van Dyk,[22] J. B. Haislip,[23] A. P. LaCluyze,[23] J. P. Moore[23] and D. Reichart[23]

[1]*Departamento de Ciencias Fisicas, Universidad Andres Bello, Avda. Republica 252, Santiago, Chile*
[2]*Department of Optics & Quantum Electronics, University of Szeged, Dóm tér 9., Szeged, 6720 Hungary*
[3]*INAF – Osservatorio Astronomico di Padova, vicolo dell'Osservatorio 5, I-35122 Padova, Italy*
[4]*INAF – Osservatorio Astrofisico di Catania, via S. Sofia 78, I-95123 Catania, Italy*
[5]*Institut de Ciències de l'Espai (CSIC-IEEC), Facultat de Ciències, Campus UAB, E-08193 Bellaterra, Spain*
[6]*Departamento de Astronomía, Universidad de Chile, Casilla 36-D, Santiago, Chile*
[7]*INAF – Osservatorio Astronomico di Capodimonte, Salita Moiariello, I-80128 Napoli, Italy*
[8]*Astrophysics Research Centre, School of Mathematics and Physics, Queen's University Belfast, Belfast BT7 1NN, UK*
[9]*Las Campanas Observatory, Carnegie Observatories, Casilla 601, La Serena, Chile*
[10]*The Oskar Klein Centre, Department of Astronomy, AlbaNova, Stockholm University, SE-10691 Stockholm, Sweden*
[11]*Kavli Institute for the Physics and Mathematics of the Universe, Todai Institutes for Advanced Study (TODIAS), University of Tokyo, 5-1-5 Kashiwanoha, Kashiwa, Chiba 277-8583, Japan*
[12]*Astronomy Department, University of Illinois at Urbana-Champaign, 1002 W. Green Street, Urbana, IL 61801, USA*
[13]*Department of Physics, University of Illinois at Urbana-Champaign, 1110 W. Green Street, Urbana, IL 61801, USA*
[14]*Taurus Hill Observatory, Härkämäentie 88, FI-79480 Kangaslampi, Finland*
[15]*Finnish Centre for Astronomy with ESO (FINCA), University of Turku, Väisäläntie 20, FI-21500 Piikkiö, Finland*
[16]*The Oskar Klein Centre, Department of Physics, Stockholm University, SE-10691 Stockholm, Sweden*
[17]*Dark Cosmology Centre, Niels Bohr Institute, University of Copenhagen, Juliane Maries vej 30, DK-2100 Copenhagen, Denmark*
[18]*Department of Physics and Astronomy, Aarhus University, Ny Munkegade 120, DK-8000 Aarhus C, Denmark*
[19]*Max Planck Institut für Astrophysik, Karl-Schwarzschild-Str. 1, D-85741 Garching bei München, Germany*
[20]*Las Cumbres Observatory Global Telescope Network, 6740 Cortona Dr., Suite 102, Goleta, CA 93117, USA*
[21]*Department of Physics, University of California, Santa Barbara, Broida Hall, Mail Code 9530, Santa Barbara, CA 93106-9530, USA*
[22]*Spitzer Science Center, California Institute of Technology, 1200 East California Boulevard, Pasadena, CA 91125, USA*
[23]*University of North Carolina at Chapel Hill, Campus Box 3255, Chapel Hill, NC 27599-3255, USA*

Accepted 2013 November 11. Received 2013 November 8; in original form 2013 October 23

ABSTRACT

We present ultraviolet, optical, near-infrared photometry and spectroscopy of SN 2009N in NGC 4487. This object is a Type II-P supernova with spectra resembling those of subluminous II-P supernovae, while its bolometric luminosity is similar to that of the intermediate-luminosity SN 2008in. We created SYNOW models of the plateau phase spectra for line identification and to measure the expansion velocity. In the near-infrared spectra we find signs indicating possible weak interaction between the supernova ejecta and the pre-existing circumstellar material. These signs are also present in the previously unpublished near-infrared spectra of SN 2008in. The distance to SN 2009N is determined via the expanding photosphere method and the standard candle method as $D = 21.6 \pm 1.1$ Mpc. The produced nickel-mass is estimated to be $\sim 0.020 \pm 0.004$ $M_{\odot}$. We infer the physical properties of the progenitor at the explosion through hydrodynamical modelling of the observables. We find the values of

⋆E-mail: ktakats@gmail.com

the total energy as $\sim 0.48 \times 10^{51}$ erg, the ejected mass as $\sim 11.5\ M_{\odot}$, and the initial radius as $\sim 287\ R_{\odot}$.

Key words: supernovae: general – supernovae: individual: SN 2008in – supernovae: individual: SN 2009N – galaxies: individual: NGC 4487.

1 INTRODUCTION

Type II supernovae (SNe) are classified on the basis of the presence of hydrogen in their spectra. SNe II-P (Barbon, Ciatti & Rosino 1979) are by far the most frequent, representing about 70 per cent of all SNe Type II (Li et al. 2011). They are characterized by nearly constant luminosities during the first period of their evolution ('plateau'). This phase lasts until their thick, initially ionized hydrogen envelopes recombine.

SNe II-P are thought to emerge from stars with a zero age main sequence mass in the range of 8–21 $M_{\odot}$ (Walmswell & Eldridge 2012). In some cases the progenitor star was directly identified in pre-explosion images as a red supergiant (RSG) star (Smartt 2009). The observational properties of these SNe, such as the peak luminosity, the plateau duration or the expansion velocity display a wide range of values.

A number of subluminous type II-P events have also been discovered and studied, including SNe 1997D (Turatto et al. 1998; Benetti et al. 2001), 2003Z (Utrobin, Chugai & Pastorello 2007), 2005cs (Takáts & Vinkó 2006; Pastorello et al. 2009), 1999br (Hamuy 2001; Pastorello et al. 2004) and 2009md (Fraser et al. 2011). These SNe have fainter absolute magnitudes, lower expansion velocities and lower nickel-masses than the majority of SNe II-P. The nature of their progenitors is still debated. In the case of SN 1997D, by modelling the observables, Turatto et al. (1998) favoured a scenario where the low ^{56}Ni-mass observed is a result of a fallback of material on to the remnant of the explosion of a massive (25–40 $M_{\odot}$) star. The hydrodynamical models of Zampieri (2007) inferred the ejecta masses of SNe 1997D and 1999br to be 14 and 10 $M_{\odot}$, respectively, while examining archival pre-explosion images Maund & Smartt (2005) estimated the mass limit for the progenitor of SN 1999br as $<15\ M_{\odot}$. In the case of SN 2003Z, the ejecta mass resulted by the modelling of Utrobin et al. (2007) was $14 \pm 1.2\ M_{\odot}$, while Zampieri (2007) estimated it to be $\sim 22\ M_{\odot}$. On the other hand, the progenitors of SNe 2005cs and 2009md were identified in archival images, and were found to have masses of $\sim$8–9 $M_{\odot}$ (Fraser et al. 2011).

In the last couple of years studies of objects that fit in between normal and subluminous SNe II-P have been published. In particular, SN 2008in had spectra very similar to those of the subluminous SNe II-P, but it had somewhat higher luminosity (Roy et al. 2011). The expansion velocities and the amount of the ejected nickel-mass were also between the typical values of normal and subluminous events. Applying the analytical relations of Litvinova & Nadezhin (1985), Roy et al. (2011) estimated the mass of the progenitor as $<20\ M_{\odot}$, while employing hydrodynamical modelling, Utrobin & Chugai (2013) obtained the value of $15.5 \pm 2.2\ M_{\odot}$. Gandhi et al. (2013) found that SN 2009js shared the characteristics of both SN 2008in and the subluminous SN 2005cs: the luminosity and the duration of its plateau were more similar to those of SN 2008in, but other properties, i.e. the ejected ^{56}Ni-mass and the explosion energy were closer to those of SN 2005cs. The mass of the progenitor was estimated in Gandhi et al. (2013) using the relations of Litvinova & Nadezhin (1985) as $11 \pm 5\ M_{\odot}$.

In this paper we present another 'intermediate-luminosity' object, SN 2009N. It was discovered by Itagaki on images taken on Jan. 24.86 and 25.62 UT in NGC 4487 (Nakano, Kadota & Buzzi 2009). They also reported that no source was visible on images taken on 2009 January 3 (limiting magnitude 18). Challis & Berlind (2009) obtained a spectrum of this SN on January 25, and classified it as a Type II SN, adding that the spectrum was a good match to that of SN 2005cs at two days after maximum.

The paper is organized as follows. In Section 2 we present the photometric data taken with ground-based telescopes through optical and near-infrared (NIR) filters, and with *Swift*/*UVOT* in the ultraviolet. In Section 3 we show the optical and NIR spectroscopic observations and study the spectral evolution. Based on the observed and measured data, the distance to SN 2009N is calculated in Section 4 via both the expanding photosphere method (EPM; Kirshner & Kwan 1974) and the standardized candle method (SCM; Hamuy & Pinto 2002). With the EPM we also estimate the explosion epoch as $t_0 = 245\,4848.1$ JD (Jan. 16.6 UT), which is adopted throughout the paper. In Section 5 the main physical parameters of the SN are inferred by hydrodynamical models. In Section 6 we summarize our results.

2 PHOTOMETRY

Optical photometric data were collected with multiple telescopes using *BVRI* and $g'r'i'z'$ filters, between days +11 and +413 after explosion (Tables B1 and B2).

The basic data reductions (bias-subtraction, overscan-correction, flat-fielding) were carried out using standard IRAF[1] routines. The brightness of the SN was measured using the point-spread function fitting technique. The calibration of the photometry was performed using standard fields (Landolt 1992; Smith et al. 2002; Landolt & Uomoto 2007) observed on photometric nights. Using these images, magnitudes for a local sequence of stars (Fig. 1, Tables B3 and B4) on the SN field were determined and used to calibrate the SN measurements. The data taken with the Liverpool Telescope were reduced using the same process, but with the QUBA pipeline, an IRAF based Python package (see Valenti et al. 2011, for details).

NIR *YJH* photometry was obtained with the Swope (RetroCam) and the du-Pont (WIRC) telescopes at Las Campanas Observatory as part of the Carnegie Supernova Project (CSP; Hamuy et al. 2006), between days +10 and +427 after explosion. Full details of the survey characteristics, data reductions and photometric processing techniques can be found in Hamuy et al. (2006), Contreras et al. (2010) and Stritzinger et al. (2011). Summarizing, NIR images were processed through a sequence of: dark subtraction, flat-field correction, sky-subtraction, non-linearity correction, then alignment and combination of dithered frames. Photometric calibration was achieved through observations of standard star fields (Persson et al.

[1] IRAF is distributed by the National Optical Astronomy Observatories, which are operated by the Association of Universities for Research in Astronomy, Inc., under the cooperative agreement with the National Science Foundation.

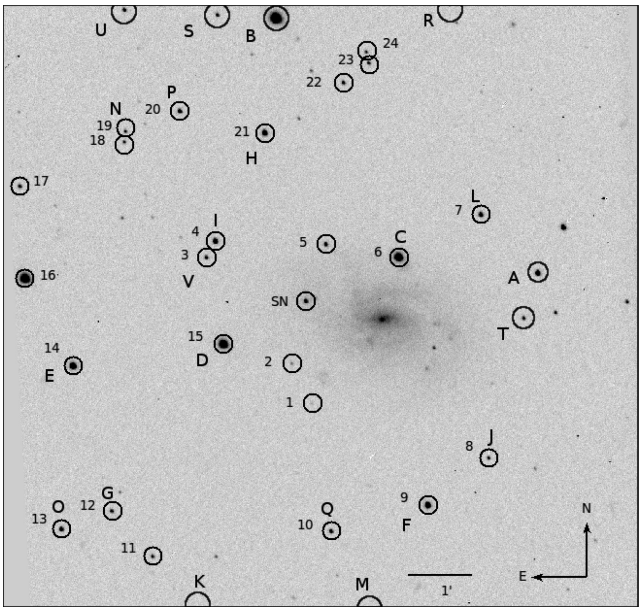

Figure 1. The field of SN 2009N in NGC 4478 obtained with one of the PROMPT telescopes in *R* band. The local comparison stars used to calibrate the optical and NIR photometry are marked with numbers and letters, respectively.

1998) and determining the magnitudes of stars on the SN field (Fig. 1, Table B5). The SN magnitudes are reported in Table B6.

The light curve (Fig. 2) shows a regular Type II-P SN, with a plateau of nearly constant luminosity in $Vv'Rr'$, lasting until about +110 d after explosion. The *B*- and g'-band light curves show constant decline from early phases, with higher decline rate during the first ∼20 d. In $Ii'YJH$ bands, the brightness increases slightly but continuously until about day +70, when it starts to decrease. At the end of the plateau the brightness drops about 2 mag in ∼3 weeks. The tail phase of SNe II-P is powered by the energy input from the radioactive decay of ^{56}Co to ^{56}Fe, so the expected decline rate is 0.98 mag/100 d for complete γ-ray trapping (Patat et al. 1994). Between days 113 and 414 we measure the decline rate as 0.85 ± 0.02 mag/100 d in the *V*, 1.02 ± 0.01 mag/100 d in the *R*, 1.03 ± 0.02 mag/100 d in the *I* band, and 1.02 ± 0.05 mag/100 d for the bolometric light curve (Section 2.3).

2.1 *Swift* photometry

SN 2009N was also observed with *Swift*/*UVOT* (Roming et al. 2005) at five epochs with all six filters. We used the HEASSOFT[2] software to co-add the images and perform aperture photometry. The count rate of the source was measured using a 3 arcsec aperture, while the coincidence loss correction was calculated using a 5 arcsec aperture. Since there are no template observations to measure the count rate originated from the galaxy, we used an aperture close to the source to measure the background level. An aperture correction was applied from the 3 arcsec to the 5 arcsec aperture, based on the average PSF available in the HEASARC Calibration Database. The zero-points from Breeveld et al. (2011) were used to convert the resulted count rate to the UVOT photometric system. The resulted magnitudes are in Table B7 and shown in Fig. 2.

[2] http://heasarc.gsfc.nasa.gov/docs/software/heasoft/

The UV light curve decreases quickly at early times, which is typical of Type II-P SNe (Dessart et al. 2008; Brown et al. 2009), while the *vv* and *bb* light curves show similar behaviour than in the Bessel *B* and *V* filters.

2.2 Reddening and colour curves

The Galactic reddening in the direction of SN 2009N is low, $E(B-V)_{\rm MW} = 0.019 \pm 0.001$ mag (Schlafly & Finkbeiner 2011). The host galaxy component of the extinction can be estimated from the equivalent width of the Na I D doublet. We have a medium-resolution spectrum, taken on day +159 after explosion (see Section 3), where the Na I D_1 and D_2 lines are resolved. We measured the equivalent widths of these lines as $EW(D1) = 0.39 \pm 0.04$ Å and $EW(D2) = 0.34 \pm 0.03$ Å. Via the relations determined by Poznanski, Prochaska & Bloom (2012) we calculated the host galaxy extinction as $E(B-V)_{host} = 0.113 \pm 0.019$ mag. Together with the Galactic component, we adopt the extinction $E(B-V)_{tot} = 0.13 \pm 0.02$ mag for SN 2009N. We must consider, however, that there is a large scatter for SNe in the EW(Na I) versus $E(B-V)$ plane (e.g. Turatto, Benetti & Cappellaro 2003; Poznanski et al. 2011), therefore the estimation of the extinction is quite uncertain.

In Fig. 3 we show the $(B-V)_0$, $(V-R)_0$, $(V-I)_0$, $(V-J)_0$ and $(V-H)_0$ colour curves of SN 2009N corrected for the reddening derived above, along with data of other Type II-P SNe. The extinction and explosion epoch of the compared SNe – which were chosen to represent a sample with large variety of physical properties – are summarized in Table 1. The optical colour evolution of SN 2009N is similar to those of other II-P SNe. The $(B-V)_0$ colour is blue at the beginning and becomes redder quickly, due to the appearance of strong metallic lines in *B* band. The evolution of the $(V-R)_0$ colour is slower. The $(V-I)_0$ colour of the six SNe shows somewhat higher scatter during the plateau phase than in the other two colours. SNe 2005cs and 2008in, along with SN 2009N, seem to be redder than the other SNe. This is more pronounced in the NIR colours, where SN 2009N is the reddest one in the sample. Since the determination of $E(B-V)$ is uncertain, we cannot rule out that we underestimated its value. However, even with significantly higher extinction the infrared colours of SN 2009N remain one of the reddest ones in the sample.

2.3 Bolometric luminosity

We calculated the quasi-bolometric luminosity of SN 2009N at those epochs when simultaneous *VRI* observations were available. If *B* band data were not taken at these epochs, they were calculated by interpolating the magnitudes from neighbouring nights using low-order polynomials. We determined the optical counterpart of the bolometric flux by correcting the observed *BVRI* magnitudes for reddening, converting them to flux densities at the effective wavelength of the filters (Bessell 1983) and integrating them using Simpson's rule. The bolometric fluxes were then converted into luminosities using the distance $D = 21.6 \pm 1.1$ Mpc (Section 4.3).

During the first 60 d of evolution *Swift* UV photometry was available (Section 2.1). We integrated the UV fluxes at each epoch, then extrapolated the resulting flux curve to the epochs of the optical photometry. Since the UV light curve decreases quickly, we assume that the UV counterpart of the bolometric flux is marginal (∼5 per cent) at later phases of the plateau (after day +80) and negligible during the nebular phase. We have NIR photometric observations

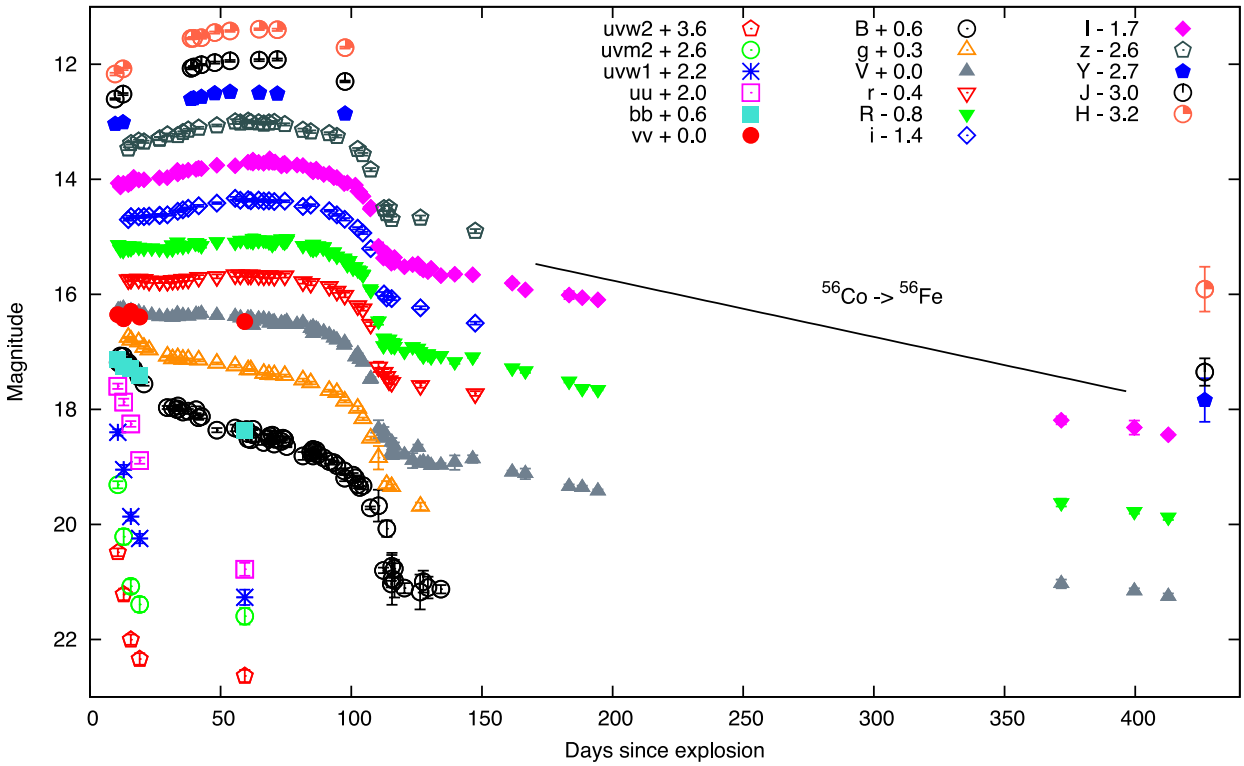

Figure 2. UV, optical, NIR light curves of SN 2009N. The explosion epoch is $t_0 = 245\,4848.1$ JD.

between days +10 and +98 after explosion (Section 2). We calculated the NIR contribution to the bolometric flux by integrating the fluxes from the red edge of the *I* to the *H* band. The flux redwards of *H* band was approximated with the Rayleigh–Jeans tail. The resulting infrared luminosities were then interpolated to the epochs of the optical observations. We calculated the bolometric luminosity curve until day +98 by adding the optical, UV and infrared luminosities.

At phases later than +98 d we lack both UV and NIR data (except at one epoch at day +427). To overcome this problem, we considered the bolometric corrections (BC) of Maguire et al. (2010b) and Bersten & Hamuy (2009). Using the data of SNe 1987A, 1999em, 2004et and 2005cs, Maguire et al. (2010b) determined BCs from both *V* and *R* bands, as a function of phase. We calculated the bolometric luminosity of SN 2009N from both *R* and *V* band photometry, which were then averaged. Comparing these to our previously calculated bolometric luminosity curve, we found that they agree excellently. Bersten & Hamuy (2009) calculated the BC as a function of colour during the plateau phase, using the bolometric light curves of three SNe (1987A, 1999em, and 2003hn) as well as the models of Eastman, Schmidt & Kirshner (1996) and Dessart & Hillier (2005). Applying their BCs to the data of SN 2009N, we found that the inferred values somewhat (by 5–10 per cent) overestimated our bolometric luminosities during the first 98 d of evolution. Since the BCs of Maguire et al. (2010b) led to luminosities that agreed well with our bolometric luminosities during the first +98 d, we used these BCs to calculate the luminosity of SN 2009N at phases later than +98 d, when UV and NIR data were not available. We also checked these BCs at the nebular phase by interpolating the *YJH* magnitudes to the epochs of the *VRI* measurements at days +372, 400, and 413, and integrating the fluxes. The resulting bolometric luminosities agreed well (within 0.1 dex) with the ones calculated with the BCs of Maguire et al. (2010b).

Fig. 4 shows the bolometric luminosity curve of SN 2009N. The observed peak luminosity was $\log L_{\rm bol} = 41.82$ erg s^{-1}. Also in Fig. 4 we compare the luminosity curve of SN 2009N with those of other SNe II-P. For better comparison we use the *BVRI* bolometric luminosities for all SNe. SN 2009N was significantly fainter than the normal SNe II-P 1999em and 2004et during the plateau phase, and about 1.5–1.8 times brighter than the subluminous SN 2005cs. Its luminosity was comparable, only slightly higher than those of the intermediate-luminosity SNe 2008in and 2009js.

3 SPECTROSCOPY

3.1 Optical spectra

Optical spectroscopic observations of SN 2009N covering the phases between days +23 and +414 after explosion were carried out with multiple telescopes. Table 2 contains the summary of the observations. The images were reduced and calibrated using standard IRAF tasks. After bias and flat corrections, the spectra were extracted. The wavelength calibration was carried out using comparison lamp spectra. Standard star spectra taken on the same night were used for the SN flux calibration, which was checked against the photometry at the nearest epoch, and – when necessary – the spectra were corrected using a scaling factor. Optical spectra were also obtained through the CSP, with the Wide Field Reimaging CCD Camera (WFCCD) and Boller & Chivens Spectrograph (BC) mounted on the du-Pont, the Low Dispersion Survey Spectrograph (LDSS3) mounted on the Magellan Clay, and the Inamori Magellan Areal Camera and Spectrograph (IMACS) mounted on the Magellan Baade telescopes at Las Campanas Observatory (Table 2). Again, overall survey techniques can be found in Hamuy et al. (2006). Spectra were processed through standard techniques of reduction, extraction and calibrations, a detailed description of which can be

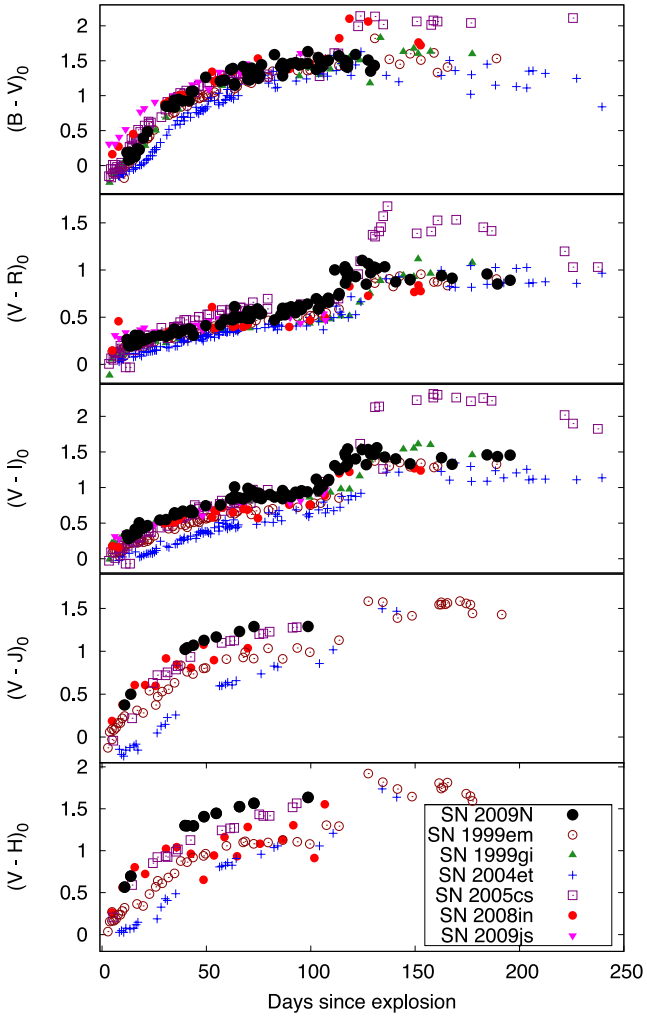

Figure 3. Evolution of $(B-V)_0$, $(V-R)_0$, $(V-I)_0$, $(V-J)_0$ and $(V-H)_0$ colours of SN 2009N, together with those of other SNe II-P: SNe 1999em, 1999gi, 2004et, 2005cs, 2008in and 2009js. The adopted reddening and the sources of photometry of these SNe are given in Table 1.

Table 1. Explosion epoch, reddening and distance of the SNe used for comparison throughout the paper.

SN	t_0 (JD)	$E(B-V)$	D (Mpc)	Ref.
1999em	245 1477.0	0.10	11.7	1,2
1999gi	245 1518.3	0.21	11.1	3
2004et	245 3270.5	0.41	4.8	4,5
2005cs	245 3549.0	0.05	8.4	6,7
2008in	245 4825.6	0.098	13.2	8
2009js	245 5115.9	0.36	21.7	9

References: (1) Hamuy et al. (2001), (2) Leonard et al. (2002a), (3) Leonard et al. (2002b), (4) Takáts & Vinkó (2012), (5) Maguire et al. (2010b), (6) Pastorello et al. (2009), (7) Vinkó et al. (2012), (8) Roy et al. (2011) and (9) Gandhi et al. (2013).

found in Folatelli et al. (2013), as applied to the SN Ia spectroscopic sample. We also obtained a medium-resolution spectrum of SN 2009N with the MagE spectrograph (Marshall et al. 2008) on the Magellan Clay 6.5 m telescope. For the MagE spectrum, the sky was subtracted from the images using the method described by Kelson (2003). We employed our own IDL routines for flux calibration and telluric line removal using the well-exposed continua of spectrophotometric standard stars (Wade & Horne 1988; Foley et al. 2004, 2009). All plateau and transition phase optical spectra are shown in Fig. 5.

The classification spectrum was taken ∼8 d after explosion by Challis & Berlind (2009). It has low signal-to-noise ratio, but the Balmer series of H I are clearly visible.[3] Using the SNID (Blondin & Tonry 2007), the spectrum was found to be similar to that of SN 2005cs two days after its maximum. Our earliest spectra of SN 2009N were taken 23, 24 and 26 d after the explosion. At that time the metallic lines already appeared in the spectrum. Next to the strong, wide Balmer series of H I, features of Fe II and Ca II were present. By day +34 features of Na I, O I, Si II, Ti II, Sc II also appeared, and remained visible throughout the plateau phase. The Na I D feature was very weak at that point, but became stronger at later phases.

We created models with SYNOW (Hatano et al. 1999; Fisher 2000) for the plateau phase spectra for line identification. The method described by Takáts & Vinkó (2012) was applied to find the set of parameters of the model that fits best the observed spectrum and to measure the photospheric velocity. An example model with line identification is shown in Fig. 6. We also measured the expansion velocities of selected lines by fitting a Gaussian to their absorption components and determining the blueshift of the minima. The line velocities of Hα, Hβ, Fe II λ5169 and Sc II λ6245 are shown in Fig. 7 together with the photospheric velocities determined via SYNOW modelling. The photospheric velocities of SN 2009N are between those of normal and subluminous SNe (Fig. 8).

An interesting detail is the appearance and strengthening of the Ba II $\lambda\lambda$5854 and 6497 lines. In Fig. 9 we enlarged the wavelength ranges around Na I D and Hα to show the evolution of these Ba II features. The Ba II lines are not visible in the first two spectra, and our SYNOW models do not show any need of their presence either. On day +40, both Ba II $\lambda\lambda$5854 and 6497 lines are very weak, but detectable, together with Ba II λ6142 (Fig. 5). By day +62 the Ba II λ6497 line is clearly visible next to Hα, while Ba II λ5854 is weak, but noticeable next to Na I. Both features become stronger and stronger throughout the plateau phase. Ba II λ5854 forms a blend with Na I, but its contribution to the line shape can be confirmed with SYNOW. These strong Ba II features seem to be typical of subluminous II-P SNe: they were detected in the spectra of e.g. SNe 2005cs (Pastorello et al. 2009), 2008in (Roy et al. 2011) and 2009md (Fraser et al. 2011).

By modelling the spectra of SN 1997D, Turatto et al. (1998) showed that the appearance of the strong Ba II lines is not due to the overabundance of Ba, an s-process element, but it is likely a temperature effect. For several elements and supernova atmosphere compositions, Hatano et al. (1999) examined how the local thermodynamic equilibrium (LTE) optical depth of one of the strongest lines of each element changes with the temperature. Their fig. 2 shows that Ba II lines appear below ∼6000 K, and the optical depth of the Ba II reference line increases very quickly as the temperature decreases. This agrees well with the evolution of Ba II features observed in SN 2009N. The temperature decreases to 6000 K around day +29 (Table 4, see also Section 4.1), and Ba II cannot be detected in the spectra taken on days +34 and +35. By the epoch of the next spectra (day +39, +40, +41), the temperature drops to ∼5700 K, and the Ba II lines start to appear, and later, with the temperature decreasing further, the features become more and more pronounced.

[3] http://www.cfa.harvard.edu/supernova/spectra/sn2009N.gif

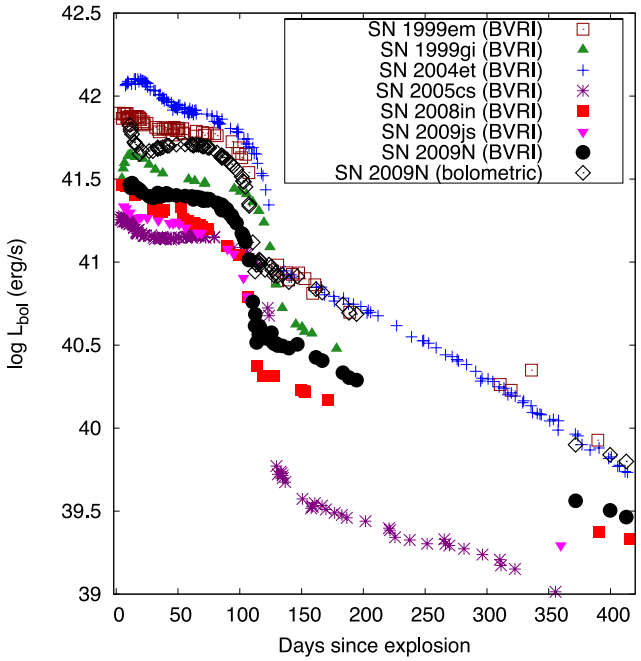

Figure 4. Comparison of the evolution of the *BVRI* quasi-bolometric luminosity of SN 2009N (filled circles) with those of other SNe II-P. The *uvoir* bolometric luminosity curve of SN 2009N is also shown (empty diamonds).

The fact that Ba II λ6497 seems to appear on the day +79 spectrum of SN 1999em (see Fig. 10), when its temperature dropped under 6000 K (see table 7 of Leonard et al. 2002a), is also in agreement with the behaviour of Ba II in SN 2009N.

In addition to their lower temperatures, subluminous SNe have lower expansion velocities, narrower spectral features, which makes Ba II lines visible at earlier phases and easier to identify.

In Fig. 10 we compare the spectrum of SN 2009N taken on day +86 to the spectra of SNe 2008in, 1999gi, 2005cs and 1999em at similar phases. The spectrum of SN 2008in – which has luminosities similar to SN 2009N (Fig. 4) – well matches that of SN 2009N; they also show similarities to that of the subluminous SN 2005cs. The spectra of the normal Type II-P SNe 1999gi and 1999em are different: the features are wider and implying higher ejecta velocities.

The nebular phase spectra of SN 2009N taken on days +158, +374 and +414, are shown in Fig. 11. The most dominant features are Hα and the Ca II IR triplet. On day +158 next to Hα and Na I D, the lines of Ba II are still strong and have P Cygni line profiles. The spectra taken on days +374 and +414 show only minor differences. They are similar to nebular phase spectra of other Type II-P SNe, such as SN 1999em, but with narrower features. Next to the strong Hα emission line and the Ca II IR triplet, features of O I and several forbidden lines can be identified, such as the [O I] 6300, 6364 Å doublet, [Fe II] 7155, 7273, 7439 Å, [Ca II] 7291,7323 Å doublet, [C I] 8727Å. [Fe II] 7273 Å appears to be somewhat stronger than in the spectra of subluminous SNe (e.g. Benetti et al. 2001; Pastorello et al. 2009).

Our two latest spectra were included in the sample of Maguire et al. (2012), who studied the nebular spectra of Type II-P SNe. Measuring the velocities from the width of the emission lines and comparing them to those of other SNe, they found that the nebular phase velocities of SN 2009N are quite low (400 − 700 km s^{-1}), and similar to those of the subluminous SN 2005cs and SN 2008bk.

Table 2. Summary of the optical spectroscopic observations.

Date	JD 240 0000+	Phase[a] (d)	Instrument set-up	Wavelength range (Å)	Resolution[b] (Å)
08/02/2009	54870.8	22.7	Magellan Clay + LDSS-3 + VPH-All	3700–10 000	7
09/02/2009	54871.8	23.7	Magellan Clay + LDSS-3 + VPH-All	3700–10 000	7
11/02/2009	54873.8	25.7	Magellan Baade + IMACS + Gri-200-15.0	3900–10 000	5
18/02/2009	54881.6	33.5	2.2-m Calar Alto + CAFOS+blue-200	3400–8900	12
19/02/2009	54882.6	34.5	2.2-m Calar Alto + CAFOS+blue-200	3400–8900	12
24/02/2009	54886.8	38.7	du Pont + WFCCD + Blue grism	3800–9100	8
25/02/2009	54887.9	39.8	du Pont + WFCCD + Blue grism	3800–9100	8
26/02/2009	54888.8	40.7	du Pont + WFCCD + Blue grism	3800–9100	8
15/03/2009	54905.8	57.7	Magellan Baade + IMACS + Gri-200-15.0	3900–10000	5
19/03/2009	54910.5	62.4	NOT + ALFOSC+grism-4	3200–9100	19
19/03/2009	54910.5	62.4	2.2-m Calar Alto + CAFOS+green-200	3790–10000	12
29/03/2009	54919.8	71.7	du Pont + WFCCD + Blue grism	3800–9100	8
03/04/2009	54924.7	76.6	du Pont + WFCCD + Blue grism	3800–9100	8
11/04/2009	54933.5	85.4	2.2-m Calar Alto + CAFOS+green-200	3790–10000	12
12/04/2009	54933.6	85.5	NOT + ALFOSC+grism-4	3200–9100	19
12/04/2009	54934.5	86.4	2.2-m Calar Alto + CAFOS+green-200	3790–10000	12
16/04/2009	54937.5	89.4	NOT + ALFOSC+grism-4	3200–9100	16
18/04/2009	54939.7	91.6	du Pont + BC + 300l/mm grating	3500–9600	8
23/04/2009	54944.8	96.7	du Pont + BC + 300l/mm grating	3500–9600	8
01/05/2009	54952.7	104.5	Magellan Clay + LDSS-3 + VPH-All	3700–10000	7
03/05/2009	54955.4	107.3	2.2-m Calar Alto + CAFOS+green-200	3790–10000	11
09/05/2009	54961.4	113.3	NOT + ALFOSC+grism-4	3200–9100	15
23/05/2009	54974.6	126.5	du Pont + BC + 300l/mm grating	3500–9600	8
24/06/2009	55006.5	158.4	Magellan Clay + MagE	3210–10350	1–2
25/01/2010	55221.8	373.7	NTT + EFOSC2+gr#16	6000–10100	14
06/03/2010	55261.8	413.7	VLT + FORS2+300V	3500–9600	10

[a]Relative to the estimated date of explosion, t_0 = 245 4848.1 JD.
[b]As measured from the full-width at half-maximum (FWHM) of the night-sky lines.

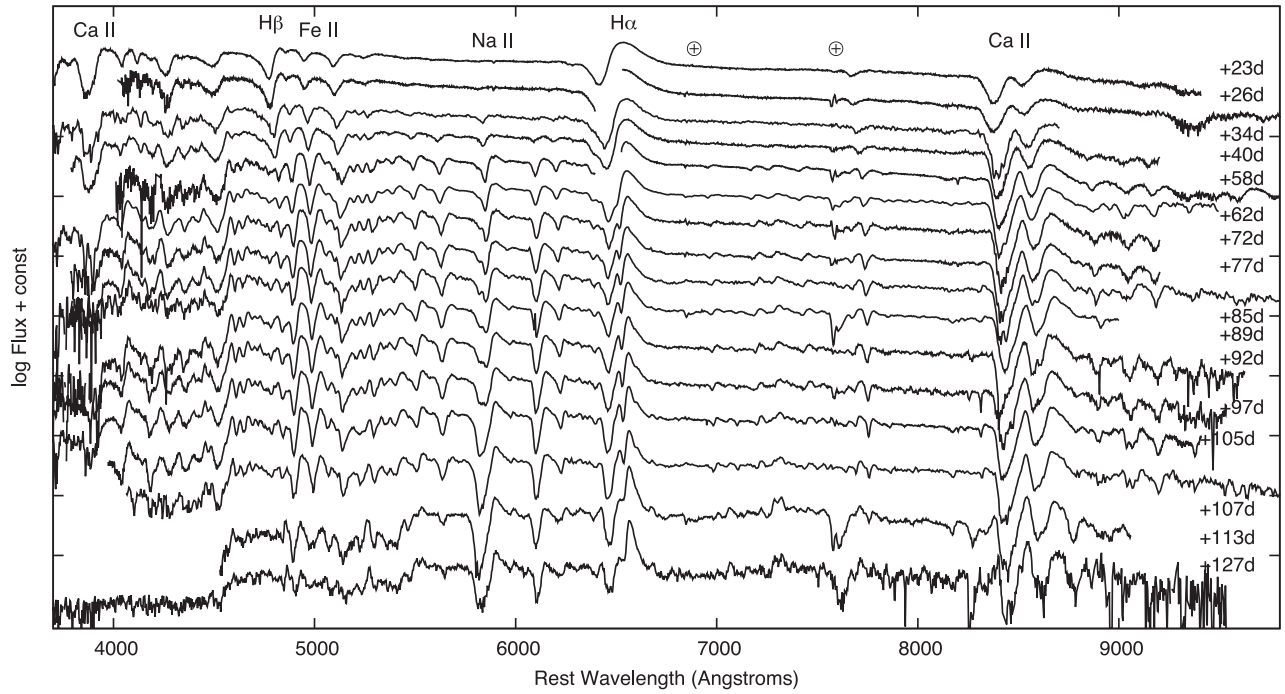

Figure 5. Spectral evolution of SN 2009N during the plateau and transition phase. Phases are relative to the estimated explosion date, $t_0 = 245\,4848.1$ JD. The approximate positions of some of the strongest features are marked to guide the eye. The positions of telluric features are marked with ⊕ symbol.

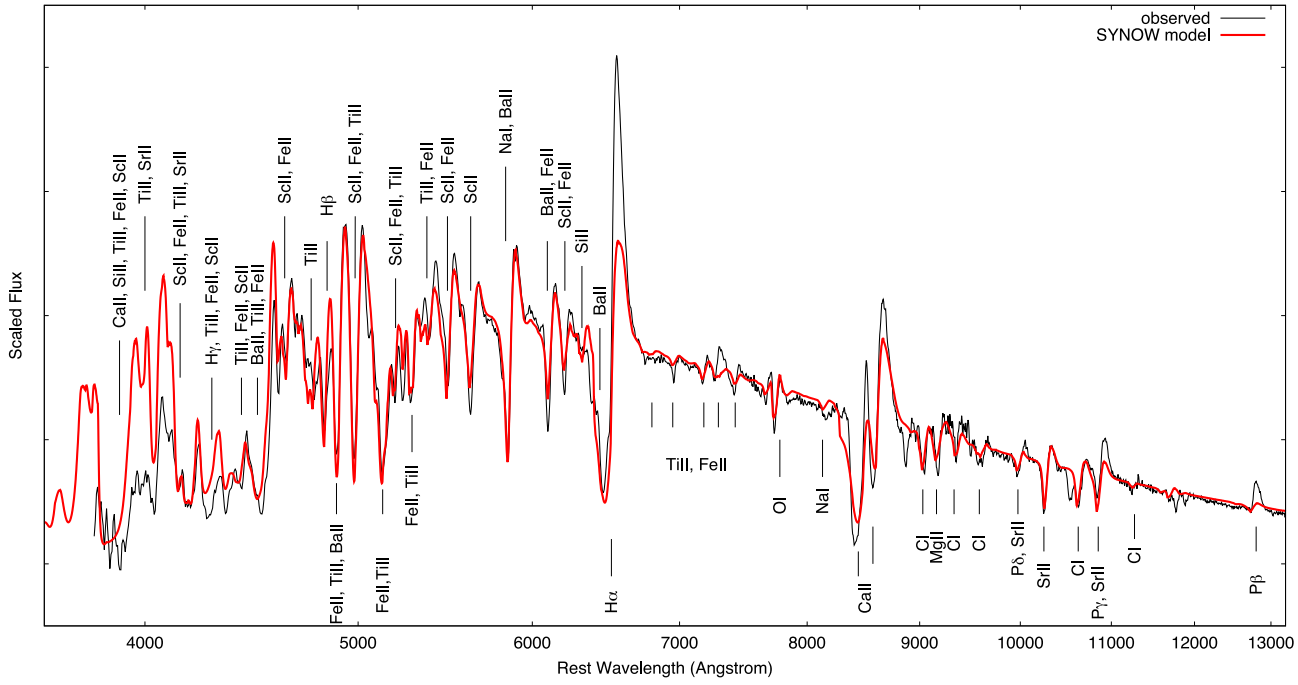

Figure 6. SYNOW model of the reddening and redshift ($z = 0.0035$) corrected, combined optical and NIR spectra, taken on days +62 and +59 with the 2.2 m Calar Alto Telescope and with NTT, respectively.

Maguire et al. (2012) also noted that the [OI] 6300 Å line profile is somewhat blueshifted at both epochs, which can be a sign of dust formation in the ejecta (see their fig. 3).

3.2 Near-infrared spectra

NIR spectra were taken at five epochs during the plateau phase with three different instruments, NTT/SOFI, VLT/ISAAC and SOAR/OSIRIS, covering the phases between days +17 and +63 after explosion. The summary of the observations can be found in Table 3. The reduction of the spectra was carried out using IRAF packages. At each epoch several pairs of spectra were taken at different positions along the slit. The pairs of images were subtracted from each other to remove the sky background. These subtracted images were then added together. The SN spectrum was extracted from the co-added image. The wavelength calibration was carried

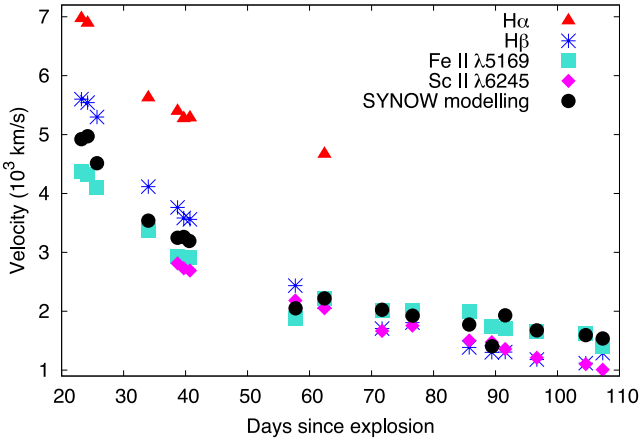

Figure 7. Expansion velocities measured from the absorption minima of selected lines, together with the photospheric velocities determined via SYNOW modelling.

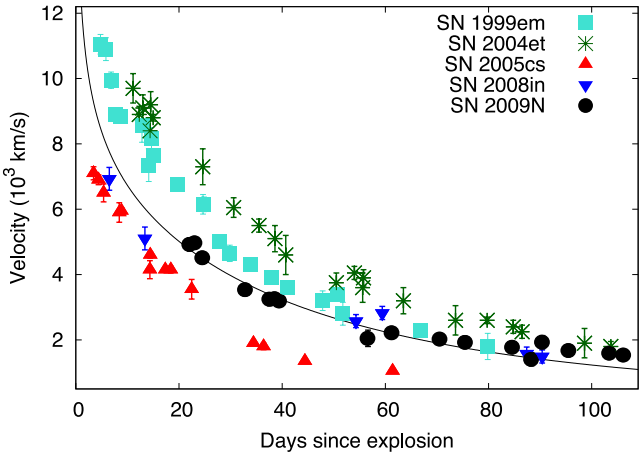

Figure 8. Comparison of the velocities of SN 2009N determined via SYNOW modelling with those of other SNe II-P (Takáts & Vinkó 2012). In order to determine the distance via EPM, the velocities of SN 2009N were extrapolated to the epochs of the photometry using the relation of Takáts & Vinkó (2012) (solid line; see Section 4.1).

out using arc lamp spectra taken at the same night as the SN spectrum. We removed the strong telluric features using the spectrum of a G-type telluric standard star observed close in time and at similar airmass as the SN. The spectrum of the telluric standard was also used for the flux calibration of the SN spectra that were later checked against the NIR photometry from the nearest epoch and corrected when necessary.

The sequence of the NIR spectra of SN 2009N is presented in Fig. 12. In the first spectrum, obtained on day +17 after the explosion, the Paschen series of H I as well as the He I feature at 2.058 μm are visible. By day +24, the strong C I λ10691 line is recognizable next to Pγ. At later phases lines of Fe II, Sr II and Ca II can be identified (Fig. 13).

Next to C I λ10691, at about 1.055 μm, an absorption feature emerged by day +47, which is not present in the spectra of normal Type II-P SNe. The reason for this could be that such objects have higher velocities and broader spectral lines, therefore since this wavelength range is dominated by the C I line, the two features – C I and the one at ∼1.055 μm – may be blended. The sample of subluminous SNe that have NIR spectra during the second half of

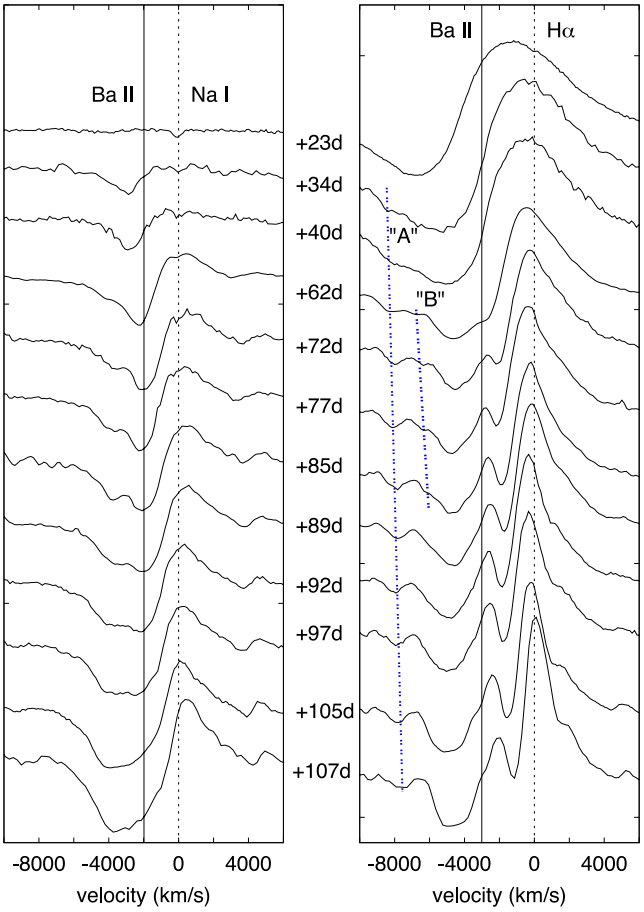

Figure 9. Evolution of the Na I D and Ba II λ5854 (left) and Hα and Ba II λ6497 (right) lines. The black vertical lines show the position of the rest wavelength of these lines. The blue dotted lines in the right panel, marked 'A' and 'B', mark the positions of the shallow absorption features that may be HV components of Hα (see also Section 3.2).

the plateau phase is quite small, and none of them has this feature present. In Fig. 14 we compare the NIR spectrum of SN 2009N taken at +59 d to that of SN 2009md (Fraser et al. 2011) at a similar phase. SN 2009md was a subluminous SN, with narrow, low-velocity spectral lines, and its NIR spectrum is similar to that of SN 2009N, but the line at 1.055 μm is not present.

Looking at our previously unpublished NIR spectra of SN 2008in (Appendix A), however, we found that they showed the same feature. In Fig. 13 the NIR spectra of the two SNe are plotted together, showing the evolution of this feature over time.

In order to try to identify the possible transition that produced this feature, we combined the optical spectrum taken on day +62 with the NIR spectrum on day +59, and used SYNOW modelling. We have found the following two possibilities.

First, we managed to model this feature at ∼1.055 μm with a high-velocity (HV) component of He I λ10830, having the velocity of ∼8000 km s^{-1}. By modelling the interaction between the ejecta and the circumstellar material (CSM) originated from average RSG wind, Chugai, Chevalier & Utrobin (2007) have shown that due to excitation of the unshocked ejecta HV features of He I λ10830 and Hα can emerge (see also Inserra et al. 2012; Inserra et al. 2013). We examined the optical spectra of SN 2009N (Section 3) to see if a HV component of Hα was also present. As Fig. 9 shows, a shallow absorption feature is visible at ∼8000 km s^{-1} (marked as 'A'). It

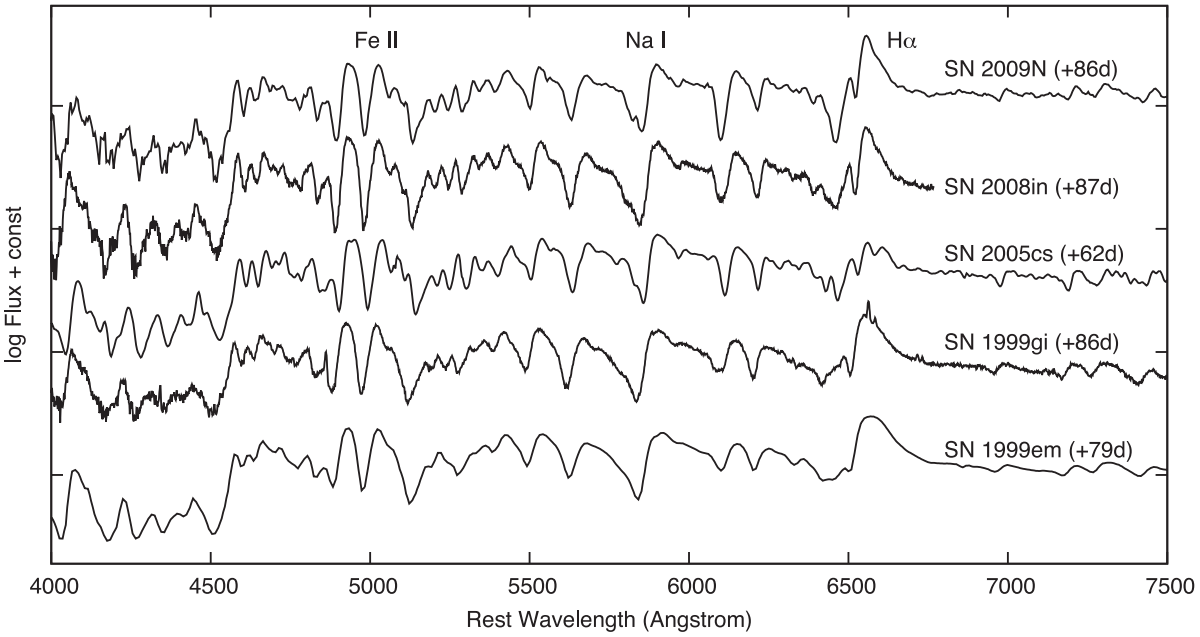

Figure 10. Comparison of the spectra of SNe 2009N and 2008in (Roy et al. 2011) with the subluminous SN 2005cs (Pastorello et al. 2009) and the normal Type II-P SNe 1999em (Leonard et al. 2002a) and 1999gi (Leonard et al. 2002b). Some of the strongest features are labelled to help the eye.

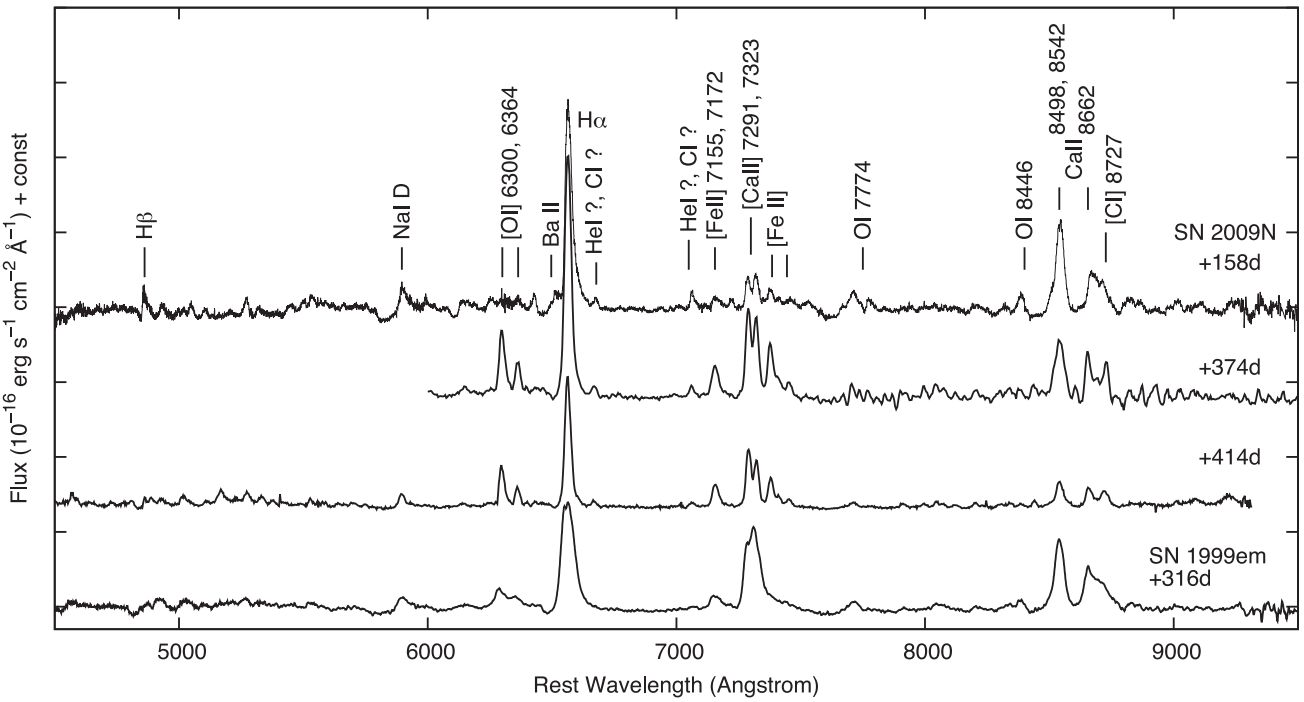

Figure 11. Nebular phase spectra of SN 2009N obtained on days +159, +374 and +414. For comparison we plotted the spectrum of SN 1999em taken on +316 d (Leonard et al. 2002a).

appears around day +39 and is present during the entire plateau phase. A smaller dip is also visible next to Hα between days +62 and +77 (marked 'B' in Fig. 9). If it is a HV component of Hα, its velocity is significantly lower and decreases more quickly. We also examined the region of Hβ, and found several weak absorption features, some of them at similar, but somewhat lower velocities as those near Hα. However, since there are many metallic lines in this region, we cannot claim for certain that any of them is a HV component of Hβ. There is no visible HV component of He I λ5876 either. The optical spectra of SN 2008in also show similar lines near Hα as in the case of SN 2009N. In fig. 8 of Roy et al. (2011) an absorption feature (marked 'C') is visible. The authors assumed it to be originated from Fe II multiplets, but they also noted that the presence of HV Hα component could not be ruled out.

We measured the velocities of the assumed HV features next to Hα and He I λ10830 in the case of both SNe 2009N and 2008in. The values are shown in Fig. 15. The velocities of HV Hα (marked 'A' in Fig. 9) and HV He I λ10830 are consistent and decrease very

Table 3. Summary of the NIR spectroscopic observations.

Date	JD 240 0000+	Phase[a] (d)	Instrument	Wavelength range μm	Resolution
03/02/2009	54 865.5	17.4	VLT+ ISAAC (SWS1-LR)	0.98–2.5	500
09/02/2009	54 872.5	24.4	NTT + SOFI (GB,GR)	0.95–1.64, 1.53–2.52	1000
04/03/2009	54 895.5	47.4	VLT+ISAAC (SWS1-LR)	0.98–2.5	500
16/03/2009	54 907.5	59.4	NTT+SOFI (GB,GR)	0.95–1.64, 1.53–2.52	1000
20/03/2009	54 911.4	63.3	SOAR+OSIRIS (Low-Res)	1.0–2.58	1200

[a]Relative to $t_0 = 245\,4848.1$ JD.

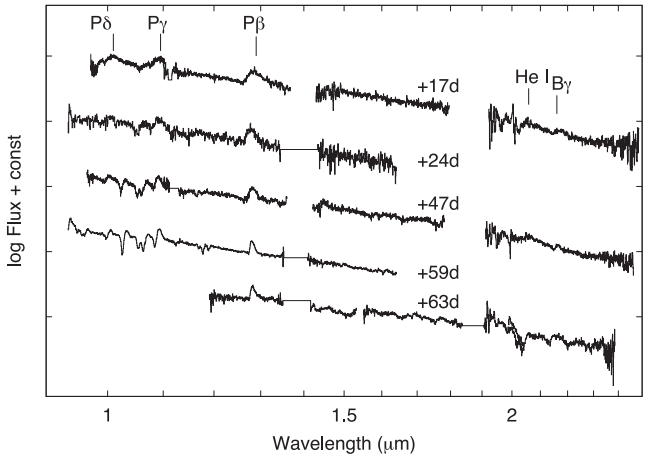

Figure 12. NIR spectra of SN 2009N. The phases are relative to the estimated date of explosion, $t_0 = 245\,4848.1$ JD.

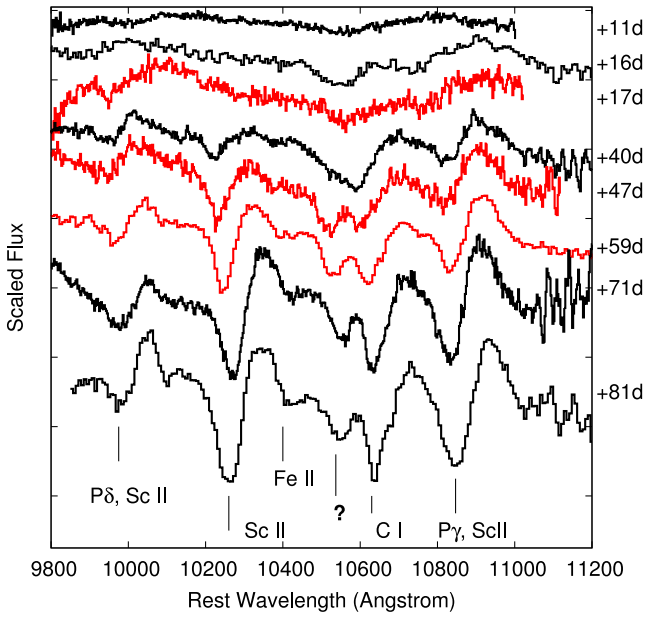

Figure 13. The emergence and evolution of the feature at about 1.055 μm (marked with '?') in the NIR spectra of SNe 2009N (red) and 2008in (black).

slowly, which supports the CSM interaction scenario. However, it seems somewhat strange that these velocities agree so well for SNe 2009N and 2008in, which suggests very similar pre-supernova evolution. For both SNe there is also a weaker feature present next to Hα with lower velocities that decrease more quickly.

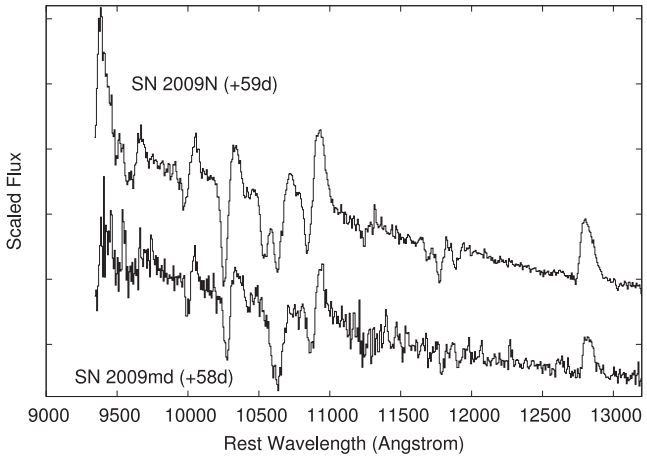

Figure 14. Comparison of the NIR spectrum of SN 2009N at +59 d after explosion with that of SN 2009md around the same phase (Fraser et al. 2011).

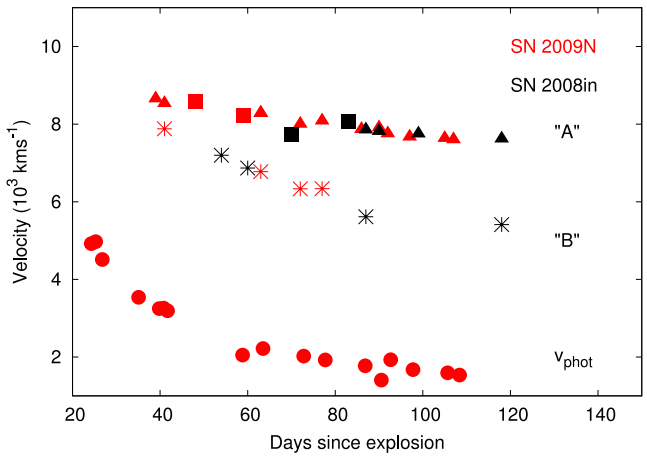

Figure 15. The velocities of the (assumed) HV features in the spectra of SNe 2009N (red) and 2008in (black): the HV Hα feature 'A' (triangles, see Fig. 9), the HV He I (squares) and the HV Hα feature 'B' (asterisks). The photospheric velocities of SN 2009N, determined via SYNOW modelling, are also shown for comparison (filled circles).

Alternatively the feature at 1.055 μm can also be modelled with Si I. However, due to the fact that Si I has several lines in the range between 1.07 and 1.09 μm that are not present in the observed spectra, our SYNOW models were unable to fit the depth of the absorption feature (Fig. 16). As in the case of the Ba II features, the presence of Si I during the second half of the plateau phase is probably a temperature effect.

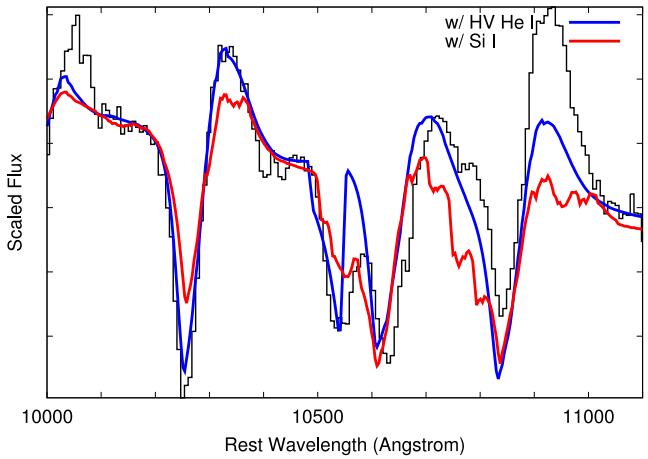

Figure 16. The wavelength range around the feature at ∼1.055 μm on day +59, together with the best-fitting SYNOW models including either Si I (red) or HV He I (blue).

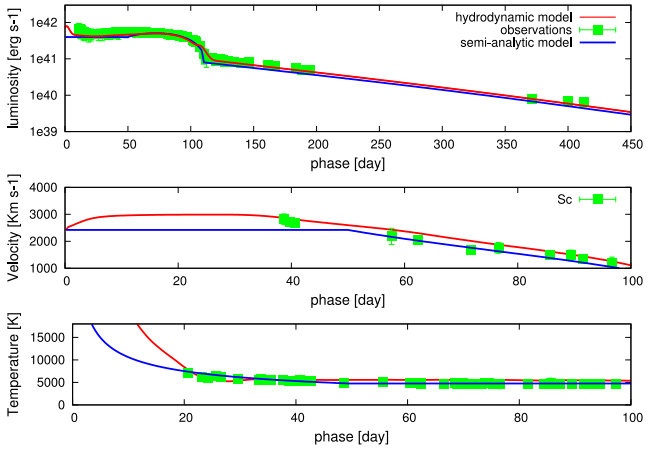

Figure 17. Comparison of the evolution of the main observables of SN 2009N with the best-fitting model computed with the general-relativistic, radiation-hydrodynamics code (total energy ∼0.48 foe, initial radius 2.0×10^{13} cm, envelope mass $\sim 11.5\,M_{\odot}$). Top, middle and bottom panels show the bolometric light curve, the photospheric velocity and the photospheric temperature as a function of time. For the sake of completeness, the best-fitting model computed with the semi-analytic code (total energy ∼0.5 foe, initial radius $\sim 1.1 \times 10^{13}$ cm, envelope mass $\sim 10\,M_{\odot}$) is also reported. The photospheric velocities were estimated from the minima of the Sc II line profiles which are considered as good tracers of the photosphere velocity in Type II SNe. The values of the photospheric temperature taken at early phase (first eight measurements corresponding to the first 15 d after the breakout of the shock wave at the stellar surface) are not included in the fit (see text for details). As for the photospheric temperature, we use the blackbody temperature derived from the blackbody fits to the spectral continuum and to the *BVRIJH* fluxes.

We plotted the observed spectrum together with the best-fitting models in both cases, i.e. including Si I or HV He I in Fig. 16, showing that the model with HV He I fits the observed spectrum better.

4 DISTANCE

The estimation of the physical properties of SNe depends on the knowledge of their distance. In the case of SNe II-P different distance measurement techniques have been developed. One of them is the EPM (Kirshner & Kwan 1974), a variant of the Baade–Wesselink method, which requires photospheric and spectroscopic monitoring throughout the first half of the plateau phase, but does not need external calibration. Another one is the SCM (Hamuy & Pinto 2002), which is based on the correlation between the SN brightness and the expansion velocity in the middle of the plateau phase. It needs less input data, but requires calibration via SNe with well-known distances. In this section we determine the distance of SN 2009N applying both mentioned methods, and then we compare and discuss the results.

4.1 Expanding photosphere method

Using the assumption that at early phases the SN has optically thick, homologously expanding ejecta, which radiates as a diluted blackbody, the EPM derives its distance by relating the apparent angular size of the photosphere to its physical radius (see for details e.g. Hamuy 2001; Leonard et al. 2002a; Dessart & Hillier 2005). By measuring the photospheric velocity and determining the angular radius θ from photometric observations on multiple epochs, the parameters t_0 and D can be derived by fitting the linear equation of $t = D \cdot (\theta / v_{\rm phot}) + t_0$.

We used SYNOW as described in Takáts & Vinkó (2012) to model the observed spectra (see also Section 3) and to determine the photospheric velocities. Since we have good photometric coverage, but not so many spectra taken during the first 50 d of evolution, we extrapolated the velocities to the epochs of the photometric measurements using the formula given in equation (3) of Takáts & Vinkó (2012). Both t_0 and the photospheric velocity on day +50 ($v_{50\rm d}$, which also depends on t_0) were fitting parameters, and the values of $t_0 = 245\,4849.4 \pm 5.7$ JD and $v_{50\rm d,\,phot} = 2588 \pm 675$ km s^{-1} were obtained. The values of the extrapolated velocities are given in Table 4 (see also Fig. 8).

We used two slightly different approaches to calculate the angular radius (θ). First, the method of Hamuy et al. (2001) was applied by minimizing the quantity of:

$$\chi^2 = \sum_{\lambda} \frac{[m_\lambda + 5\log(\theta\zeta(T)) - b_\lambda(T)]}{\sigma_m^2}, \qquad (1)$$

where m_λ is the dereddened apparent magnitude in the filter with the central wavelength λ, σ_m is the photometric error of m_λ, $b_\lambda(T)$ is the syntetic magnitudes of the blackbody flux at temperature T, $\zeta(T)$ is the flux dilution factor. In this way both θ and T are determined simultaneously. The *BVI* filter combination was taken into account. We refer to this version as 'multicolour'.

We also applied EPM in a 'bolometric' way (Vinkó et al. 2004). In this case the angular radius was calculated as

$$\theta = \sqrt{\frac{F_{\rm bol}}{\zeta^2(T)\sigma T^4}}. \qquad (2)$$

We used the bolometric fluxes determined in Section 2.3 ($F_{\rm bol}$), while the temperatures were obtained by fitting blackbody curves to the fluxes measured in the *BVRIJH* bands.

To calculate the distance, we adopted the $\zeta(T)$ dilution factors of Dessart & Hillier (2005). Table 4 contains the derived θ, T and ζ values for both methods along with the extrapolated $v_{\rm phot}$ velocities.

Using the 'multicolour' method the inferred distance is $D_{\rm m} = 22.96 \pm 2.85$ Mpc, while for the epoch of explosion we obtained $t_{0,\,\rm m} = 245\,4847.0 \pm 2.2$ JD. With the 'bolometric' version the results are $D_{\rm b} = 23.64 \pm 2.65$ Mpc and $t_{0,\,\rm b} = 245\,4848.9 \pm 1.5$ JD. We adopted the weighted mean of the results of the two versions

Table 4. Quantities derived in EPM: angular size (θ), temperature (T) and dilution factors (ζ) from the models of Dessart & Hillier (2005) along with the extrapolated velocities.

	'Bolometric'			'Multicolour'			Extrapolated velocities
JD (240 0000+)	θ (10^8 $\frac{\text{km}}{\text{Mpc}}$)	T (K)	ζ	θ (10^8 $\frac{\text{km}}{\text{Mpc}}$)	T (K)	ζ	v_{phot} (km s^{-1})
54858.9	3.20	9006	0.540	3.47	8998	0.588	6843
54859.7	2.48	10042	0.431	3.15	9935	0.548	6659
54859.8	2.93	9252	0.511	3.38	9050	0.589	6638
54860.9	2.50	9996	0.451	3.44	9152	0.622	6403
54862.8	2.84	8988	0.546	3.51	8737	0.676	6017
54862.8	2.78	9137	0.535	3.71	8192	0.714	6021
54863.8	2.96	8691	0.585	3.63	8505	0.719	5843
54864.8	3.17	8212	0.646	3.96	7768	0.807	5675
54866.8	3.50	7521	0.754	3.99	7569	0.861	5370
54868.8	3.68	7017	0.836	4.11	7188	0.935	5095
54874.7	5.03	4401	1.318	4.37	6581	1.147	4413
54877.7	4.33	5830	1.216	4.61	6016	1.296	4122
54881.6	4.59	5544	1.402	5.46	5207	1.667	3790
54881.7	4.48	5655	1.371	4.73	5979	1.448	3780
54881.8	4.48	5694	1.373	4.84	5960	1.486	3775
54883.7	4.56	5538	1.455	4.91	5701	1.570	3624
54885.7	4.59	5508	1.528	4.93	5791	1.641	3478
54888.8	4.65	5497	1.644	4.91	5928	1.739	3272
54889.7	4.74	5292	1.707	5.09	5554	1.837	3211
54890.7	4.71	5351	1.732	5.09	5382	1.873	3147
54896.7	4.90	4992	2.019	5.37	5198	2.212	2810
54903.7	4.88	5019	2.281	5.37	5195	2.512	2477

of EPM, $D_{EPM} = 23.31 \pm 1.94$ Mpc ($\mu = 31.83 \pm 0.18$ mag) and $t_0 = 245\,4848.1 \pm 1.2$ JD as the EPM distance to SN 2009N and the epoch of its explosion (which date we use throughout the paper), respectively.

The distances determined via EPM depend heavily on the $\zeta(T)$ dilution factors that are calculated from atmosphere models. Currently there are two sets of models that can be used for this purpose, published by Eastman et al. (1996) and Dessart & Hillier (2005). The $\zeta(T)$ curves derived from these two model sets, however, differ significantly, those of Eastman et al. (1996) being systematically lower, therefore leading to lower distances (as was discussed in Dessart & Hillier 2005). In the case of SN 2009N the difference in the distance is ∼14 per cent.

4.2 Standardized candle method

The SCM was originally proposed by Hamuy & Pinto (2002) and has been refined several times (Hamuy 2005; Nugent et al. 2006; Poznanski et al. 2009; Olivares et al. 2010). In this section we use multiple versions.

First we apply the version of Poznanski et al. (2009). Using the measured brightness, expansion velocity and well-known distance of a sample of 34 SNe, they calibrated the equation

$$\mathcal{M}_{\mathcal{I}} - \alpha \cdot \log\left(\frac{v_{\text{Fe}}(50\text{d})}{5000}\right) + R_I((V-I) - (V-I)_0) - m_I = -5 \cdot \log(H_0 D) \quad (3)$$

where $\mathcal{M}_{\mathcal{I}} = -1.615 \pm 0.08$, $\alpha = 4.4 \pm 0.6$, $R_I = 0.8 \pm 0.3$ and $(V-I)_0 = 0.53$ mag. We measured the I-band magnitude of SN 2009N on day +50 as $m_I = 15.440 \pm 0.015$ mag, the colour as $(V-I) = 0.850 \pm 0.025$ mag, and $v_{\text{Fe}}(50\text{d}) = 2448 \pm 300$ km s^{-1}. We adopt the latest value of the Hubble constant, that was determined by the Planck collaboration: $H_0 = 67.3 \pm 1.2$ km s^{-1}Mpc^{-1} (Planck collaboration 2013). The obtained distance is $D_{\text{SCM, 1}} = 21.01 \pm 2.86$ Mpc

Maguire et al. (2010a) extended the technique by using NIR photometry and showed that in *JHK* bands the scatter in the Hubble diagram is lower than in the optical. They used the same formula as Poznanski et al. (2009) (equation 3). Their calibration in J band – which had the lowest scatter among the three bands – led to the values of $\mathcal{M}_{\mathcal{J}} = -2.532 \pm 0.250$ mag and $\alpha = 6.33 \pm 1.20$. Maguire et al. (2010a) opted to calculate with the value of $R_V = 1.5$, obtained by Poznanski et al. (2009), instead of using it as a fitting parameter. In the case of SN 2009N, +50 d after the explosion we measured $m_J = 15.198 \pm 0.020$, $(V-J) = 1.14 \pm 0.04$ mag and again used the velocity $v_{\text{Fe}}(50\text{d}) = 2448 \pm 300$ km s^{-1}. The calculated distance is $D_{\text{SCM, 2}} = 20.82 \pm 4.35$ Mpc.

Both of the above methods rely on data taken on day +50 after explosion. However, in many cases the date of the explosion cannot be determined accurately. And even though the brightness does not change significantly around day +50, the velocity does; a few days uncertainty in the epoch of explosion can change the measured $v(50\text{d})$ by ±200–250 km s^{-1}. In the case of SN 2009N, 200 km s^{-1} difference alone would change the distance by ∼8 per cent. A solution to this problem was proposed in Olivares et al. (2010), who used an epoch calculated relative to the middle of the transition from the plateau to the tail.

Olivares et al. (2010) examined the data of 37 nearby II-P SNe, and applied the same expression as Hamuy & Pinto (2002):

$$m + \alpha \log(v_{\text{Fe}}/5000) - \beta(V-I) = 5 \log H_0 D + zp, \quad (4)$$

but using the magnitudes and velocities measured 30 d before the middle of the transition phase (t_{PT}). The values of α, β and zp can be found in table 6 of Olivares et al. (2010) for the

Table 5. Comparison of the distances obtained with different methods in this paper and in Tully (1988). Their weighted mean is also included.

Method	Distance (Mpc)	Distance modulus (mag)	Ref.
Tully–Fisher	19.9 (4.0)	31.49 (0.44)	Tully (1988)
EPM	23.3 (1.9)	31.84 (0.18)	This paper
SCM	21.0 (1.4)	31.61 (0.14)	This paper
Average	21.6 (1.1)	31.67 (0.11)	

filters *BVI*. In the case of SN 2009N we determined the middle of the transition by fitting the model function of Elmhamdi, Chugai & Danziger (2003) to the light curve as $t_{\rm PT} = 109 \pm 2$ d after explosion. On day $t_{\rm PT} - 30$ we measured the values of $m_B = 18.100 \pm 0.090$, $m_V = 16.470 \pm 0.016$, $m_I = 15.452 \pm 0.007$ mag and $v_{\rm Fe} = 1822 \pm 150$ km s^{-1}. We determined the distance for all three bands, and calculated their weighted mean. This way we obtained a distance of $D_{\rm SCM,\,3} = 21.11 \pm 1.65$ Mpc.

The distances determined with the three versions of SCM agree quite well. We conclude their weighted mean, $D_{\rm SCM} = 21.02 \pm 1.36$ Mpc ($\mu = 31.61 \pm 0.14$ mag), as the SCM distance to SN 2009N. Note that SCM has multiple uncertainties. It requires external calibration using SNe with well-known distances and depends on the value of H_0. Adopting, for example, $H_0 = 73$ km s^{-1}Mpc^{-1} (Freedman & Madore 2010) instead of $H_0 = 67.3$ km s^{-1}Mpc^{-1} would lower the SCM distance of SN 2009N by ∼8 per cent.

4.3 Average distance

The distances derived via EPM and SCM differ significantly, $D_{\rm EPM}$ being higher by ∼10 per cent than $D_{\rm SCM}$. Olivares et al. (2010) compared the SCM and EPM distances of SNe that were both in their sample and in the sample of Jones et al. (2009). They found that the EPM distances (using the atmosphere models of Dessart & Hillier 2005) are systematically higher than those calculated via SCM.

The distance of NGC 4487, the host galaxy of SN 2009N, was determined by Tully (1988) as $D_{\rm TF} = 19.9 \pm 4.0$ Mpc ($\mu = 31.49 \pm 0.4$ mag) from the Tully–Fisher relation. This value is in agreement with our findings. On the other hand, the distance of the host galaxy derived from the redshift is significantly lower. After correcting for the Virgo infall a value of 15.3 ± 0.9 Mpc can be obtained[4] (with $H_0 = 67.3$ kms^{-1}Mpc^{-1}, as in the previous section). In the case of such nearby galaxies, peculiar motions can play an important role, and can explain the difference.

By calculating the weighted average of the SCM, EPM and Tully–Fisher distances, and excluding the Hubble flow distance (Table 5), we determined our best estimate of the distance to NGC 4487 as $D = 21.6 \pm 1.1$ Mpc ($\mu = 31.67 \pm 0.11$).

5 PHYSICAL PARAMETERS

Based on our observations and the distance determined in the previous section, we infer some of the physical parameters of the progenitor star and the explosion of SN 2009N.

[4] HyperLeda, http://leda.univ-lyon1.fr/

The ^{56}Ni mass produced during the explosion was estimated from the tail luminosity. Using equation (2) in Hamuy (2003), we estimated the nickel mass to be $M_{\rm Ni} = 0.020 \pm 0.004$ M$_\odot$.

With the same well-tested approach adopted for other observed CC-SNe (e.g. SNe 2007od, 2009bw and 2009E; see Inserra et al. 2011, 2012; Pastorello et al. 2012), we evaluated the main physical properties of the progenitor of SN 2009N at the explosion (i.e. the ejected mass, the progenitor radius and the explosion energy) through the hydrodynamical modelling of the main observables (i.e. bolometric light curve, evolution of line velocities and continuum temperature at the photosphere).

According to this approach, a simultaneous χ^2 fit of the above-mentioned observables against model calculations was performed. Two codes were employed for the computation of the models: (1) the first one is a semi-analytic code where the energy balance equation is solved for a homologously expanding envelope of constant density (Zampieri et al. 2003; Zampieri 2007); (2) the second is a new general-relativistic, radiation-hydrodynamics Lagrangian code presented in Pumo, Zampieri & Turatto (2010) and Pumo & Zampieri (2011), which is able to simulate the evolution of the physical properties of the CC SN ejecta and the behaviour of the main observables from the breakout of the shock wave at the stellar surface up to the nebular stage. The distinctive features of this new code are: (a) an accurate treatment of radiative transfer coupled to hydrodynamics, (b) a fully implicit Lagrangian approach to the solution of the coupled non-linear finite difference system of general-relativistic, radiation-hydrodynamics equations, and (c) a description of the evolution of ejected material which takes into account both the gravitational effects of the compact remnant and the heating effects linked to the decays of the radioactive isotopes synthesized during the SN explosion.

The semi-analytic code is used to carry out a preparatory study aimed at constraining the parameter space describing the SN progenitor at the explosion. The results of such study are exploited to guide the more realistic, but time-consuming model calculations performed with the general-relativistic, radiation-hydrodynamics code.

We note that modelling with both codes is appropriate, since the emission of SN 2009N is dominated by the expanding ejecta. However, in performing the χ^2 fit, we do not include the observational data taken at early phase (first ∼10–20 d after explosion). This is approximately the time needed for the early bolometric light curve to relax to the plateau (see e.g. Tomasella et al. 2013). We do not attempt to model this phase because during it all the observables are significantly affected by emission from the outermost shell of the ejecta, which is not in homologous expansion (cf. Pumo & Zampieri 2011). The structure, evolution and emission properties of this shell are not well reproduced in our simulations because at present we adopt an 'ad hoc' initial density profile, not consistently derived from a post-explosion calculation. Future plans involve implementing more 'realistic' density profiles in the simulations.

The shock breakout epoch, the bolometric luminosity, the photospheric velocity and the photospheric temperature were necessary to perform the comparison with model calculations (see Fig. 17). The agreement between our modelling and the observations is reasonably good apart from the early evolution of the photometric velocity. As mentioned before, the reason for this difference is due to the 'ad hoc' initial density profile used in our simulations, which does not reproduce correctly the radial profile in the outermost shells of the ejecta formed after shock breakout. For this reason, we omit the early phase data from the fit. However, it should be noted that such omission does not affect the results significantly, the modelling

provides a reliable estimate of the main physical properties of the SN progenitor.

Assuming a ^{56}Ni mass of $0.020 \pm 0.004\,M_{\odot}$, the best-fitting model calculated with the general-relativistic, radiation-hydrodynamics code returned values of total (kinetic plus thermal) energy of ∼0.48 foe, initial radius of $\sim 2.0 \times 10^{13}$ cm ($\sim 287\,R_{\odot}$) and envelope mass of $\sim 11.5\,M_{\odot}$.

Adding the mass of a compact remnant ($\sim$1.5–2 $M_{\odot}$) to that of the ejected material, the estimated mass of the progenitor of SN 2009N at the explosion is $\sim$ 13–13.5 $M_{\odot}$, which is consistent with the mass range of the RSG precursors of SNe II-P (e.g. Smartt et al. 2009). Examining the pre-explosion images of SN 2009N, the upper limit for the progenitor mass was determined as $M_{\rm ZAMS} < 16\,M_{\odot}$ (see Maguire et al. 2012, and the references therein). The initial radius, however, is quite small for a RSG star; it is more consistent with that of a yellow supergiant.

The estimated physical parameters of SN 2009N are in between those of the subluminous and normal SNe II-P. The ejected ^{56}Ni mass (0.020 $M_{\odot}$) is higher than that of the subluminous SNe 2005cs (0.003–0.004 $M_{\odot}$; Pastorello et al. 2009) and 2003Z (0.0063 $M_{\odot}$; Utrobin et al. 2007), but lower than that of the normal II-P SN 1999em (0.036 $M_{\odot}$; Utrobin 2007). Similarly, the explosion energy (∼0.48 foe) is in between the typical values of the subluminous (e.g. 0.2–0.4 foe and 0.245 foe for SNe 2005cs and 2003Z, respectively) and the normal SNe II-P (e.g. 1.3 foe for SN 1999em; Zampieri 2007). The initial radii and progenitor masses of SNe 2009N and 2003Z are alike, although the explosion energy of SN 2003Z was about half of that of SN 2009N (Utrobin et al. 2007).

The observational properties of SN 2009N are very similar to those of SN 2008in. The estimated ^{56}Ni masses are also in good agreement. Roy et al. (2011) used the semi-analytical formulae of Litvinova & Nadezhin (1985) to estimate the physical parameters of the explosion and the progenitor of SN 2008in. They found that the progenitor was a compact star with $R_{\rm ini} \approx 127\,R_{\odot}$ and $M_{\rm ej} \approx 17\,M_{\odot}$. This radius is lower and the ejected mass is higher than those of SN 2009N. The explosion energies of the two SNe are similar. Using hydrodynamical modelling, Utrobin & Chugai (2013) also determined the parameters of SN 2008in. They obtained the ejecta mass of $13.6 \pm 1.9\,M_{\odot}$ and the explosion energy of 0.51 ± 0.34 foe, which are close to the parameters inferred for SN 2009N. On the other hand, they estimated the radius of the progenitor of SN 2008in to be significantly larger than that of Roy et al. (2011), viz. $R_{\rm ini} = 570 \pm 100\,R_{\odot}$.

6 SUMMARY

In this paper we present ultraviolet, optical and NIR photometry of SN 2009N together with optical and NIR spectra. The spectral and photometric evolution is similar to that of the intermediate-luminosity SN II-P, 2008in (Roy et al. 2011). The optical spectra show narrow features with low velocities, typical of subluminous SNe II-P. We examined the evolution of the strong Ba II λλ5854 and 6497 lines, which are mainly detected in the spectra of subluminous SNe II-P. The bolometric luminosity during the plateau phase is in between those of the subluminous and normal SNe II-P.

The NIR spectra of SN 2009N contain the usual features typical of SNe II-P, except for the appearance of a feature at ∼1.055 μm on day +48 after explosion. We also show that this feature is present in – previously unpublished – NIR spectra of SN 2008in. Creating SYNOW models of the spectra we found that this line is probably due to HV He I λ10830, although we cannot rule out the identification as Si I either. The presence of HV He I, together with HV component of Hα, can be a sign of weak interaction of the ejecta with CSM (Chugai et al. 2007).

We estimated the distance to SN 2009N using multiple versions of both the EPM and the SCM. As a result we determined the distance as $D = 21.6 \pm 1.1$ Mpc ($\mu = 31.67 \pm 0.11$). The produced nickel mass is estimated to be $0.020 \pm 0.004\,M_{\odot}$. Physical properties of the progenitor at the explosion were determined through hydrodynamical modelling. The total explosion energy (∼0.48 foe) is in between the values typical of subluminous and normal SNe II-P. The presupernova mass ($\sim$ 13–13.5 $M_{\odot}$) is consistent with that of RSG stars, while small estimated radius at the time of the explosion ($R_{\rm ini} \approx 287\,R_{\odot}$) can point to a YSG star more than to a RSG. The directly identified progenitors of normal SNe II-P, however, are all RSG stars (Smartt et al. 2009), the only object for which the possibility of a YSG progenitor arose was SN 2008cn, a high-luminosity SNe II-P (Elias-Rosa et al. 2009).

ACKNOWLEDGEMENTS

KT acknowledges support by the Gemini-Conicyt project 32110024. KT, GP, JA, FB, RC, MH and FF acknowledge support from Millennium Center for Supernova Science (P10-064-F), with input from Fondo de Innovación para la Competitividad, del Ministerio de Economia, Fomento y Turismo de Chile. This project has been supported by the Hungarian OTKA grant NN 107637 and by the European Union together with the European Social Fund through the TÁMOP 4.2.2/B-10/1-2010-0012 grant. We acknowledge the TriGrid VL project and the INAF-Astronomical Observatory of Padua for the use of computer facilities. MLP, AP and SB acknowledge support from the PRIN-INAF 2011 Transient Universe: from ESO Large to PESSTO (P.I. S. Benetti). NER acknowledges financial support by the MICINN grant AYA2011-24704/ESP, by the ESF EUROCORES Program EuroGENESIS (MINESCO grant EUI2009-04170), and from the European Union Seventh Framework Programme (FP7/2007-2013) under grant agreement n. 267251. FB, JA and FF acknowledge support from CONICYT through FONDECYT grants 3120227, 3110142 and 3110042, respectively. FF acknowledges partial support from Comite Mixto ESO-GOBIERNO DE CHILE. RC acknowledges support by CONICYT through Programa Nacional de Becas de Postgrado grant D-2108082, and by the Yale-Chile fellowship in astrophysics. GL is supported by the Swedish Research Council through grant No. 623-2011-7117. MS gratefully acknowledges generous support provided by the Danish Agency for Science and Technology and Innovation realized through a Sapere Aude Level 2 grant.

This work is partially based on observations made with ESO Telescopes at the La Silla and Paranal Observatories under programme IDs 084.D-0261 and 082.A-0526, and on observations of the European supernova collaboration involved in the ESO-NTT large programme 184.D-1140 led by Stefano Benetti. This research is based in part on observations made with the Liverpool Telescope operated on the island of La Palma by Liverpool John Moores University in the Spanish Observatorio del Roque de los Muchachos of the Instituto de Astrofisica de Canarias with financial support from the UK Science and Technology Facilities Council; the Nordic Optical Telescope, operated on the island of La Palma jointly by Denmark, Finland, Iceland, Norway, and Sweden, in the Spanish Observatorio del Roque de los Muchachos of the Instituto de Astrofisica de Canarias; the SMARTS Consortium 1.3 m telescope and the Prompt Telescopes located at Cerro Tololo Inter-American Observatory (CTIO), Chile; the 1.5 m telescope located at Palomar Observatory, USA; the 2.2 m telescope of the Calar Alto

Observatory (Sierra de Los Filabres, Spain); the Southern Astrophysical Research (SOAR) telescope, which is a joint project of the Ministério da Ciência, Tecnologia, e Inovação (MCTI) da República Federativa do Brasil, the U.S. National Optical Astronomy Observatory (NOAO), the University of North Carolina at Chapel Hill (UNC), and Michigan State University (MSU); the 2.5 m du Pont Telescope and the 6.5 m Magellan Telescopes located at Las Campanas Observatory, Chile. We are grateful to the staffs at these observatories for their excellent assistance with the observations.

This research has made use of the NASA/IPAC Extragalactic Database, the HyperLeda data base, NASA's Astrophysics Data System. The availability of these services is gratefully acknowledged.

We thank Rupak Roy for sending us the optical spectra of SN 2008in and Morgan Fraser for the NIR spectra of SN 2009md. We also thank the referee, V. P. Utrobin, for the thorough review of the paper.

REFERENCES

Barbon R., Ciatti F., Rosino L., 1979, A&A, 72, 287
Benetti S. et al., 2001, MNRAS, 322, 361
Bersten M. C., Hamuy M., 2009, ApJ, 701, 200
Bessell M. S., 1983, PASP, 95, 480
Blondin S., Tonry J. L., 2007, ApJ, 666, 1024
Breeveld A. A., Landsman W., Holland S. T., Roming P., Kuin N. P. M., Page M. J., 2011, in McEnery J. E., Racusin J. L., Gehrels N., eds, AIP Conf. Ser. Vol. 1358, An Updated Ultraviolet Calibration for the Swift/UVOT. Am. Inst. Phys., New York, p. 373
Brown P. J. et al., 2009, AJ, 137, 4517
Challis P., Berlind P., 2009, CBET, 1673, 2
Chugai N. N., Chevalier R. A., Utrobin V. P., 2007, ApJ, 662, 1136
Contreras C. et al., 2010, AJ, 139, 519
Dessart L., Hillier D. J., 2005, A&A, 439, 671
Dessart L. et al., 2008, ApJ, 675, 644
Eastman R. G., Schmidt B. P., Kirshner R., 1996, ApJ, 466, 911
Elias-Rosa N. et al., 2009, ApJ, 706, 1174
Elmhamdi A., Chugai N. N., Danziger I. J., 2003, A&A, 404, 1077
Fisher A. K., 2000, PhD thesis, The University of Oklahoma
Folatelli G. et al., 2013, ApJ, 773, 53
Foley R. J. et al., 2004, PASP, 115, 1220
Foley R. J. et al., 2009, AJ, 138, 376
Fraser M. et al., 2011, MNRAS, 417, 1417
Freedman W. L., Madore B. F., 2010, ARA&A, 48, 673
Gandhi P. et al., 2013, ApJ, 767, 166
Hamuy M., 2001, PhD thesis, The University of Arizona
Hamuy M., 2003, ApJ, 582, 905
Hamuy M., 2005, in Marcaide J.-M., Weiler K. W., eds, IAU Colloq. 192: Cosmic Explosions, On the 10th Anniversary of SN1993J. Springer, Berlin, p. 535
Hamuy M., Pinto P. A., 2002, ApJ, 566, L63
Hamuy M. et al., 2001, ApJ, 558, 615
Hamuy M. et al., 2006, PASP, 118, 2
Hatano K., Branch D., Fisher A., Millard J., Baron E., 1999, ApJS, 121, 233
Inserra C. et al., 2011, MNRAS, 417, 261
Inserra C. et al., 2012, MNRAS, 422, 1122
Inserra C. et al., 2013, A&A, 555, A142
Jones M. I. et al., 2009, ApJ, 696, 1176
Kelson D. D., 2003, PASP, 115, 688
Kirshner R. P., Kwan J., 1974, ApJ, 193, 27
Landolt A. U., 1992, AJ, 104, 340
Landolt A. U., Uomoto A. K., 2007, AJ, 133, 768
Leonard D. C. et al., 2002a, PASP, 114, 35
Leonard D. C. et al., 2002b, AJ, 124, 2490
Li W. et al., 2011, MNRAS, 412, 1441
Litvinova I. Y., Nadezhin D. K., 1985, SvA, 11, 145
Maguire K., Kotak R., Smartt S. J., Pastorello A., Hamuy M., Bufano F., 2010a, MNRAS, 403, L11
Maguire K. et al., 2010b, MNRAS, 404, 981
Maguire K. et al., 2012, MNRAS, 420, 3451
Marshall J. L. et al., 2008, Proc. SPIE, 7014, 169
Maund J. R., Smartt S. J., 2005, MNRAS, 360, 288
Nakano S., Kadota K., Buzzi L., 2009, CBET, 1670, 1
Nugent P. et al., 2006, ApJ, 645, 841
Olivares E. F. et al., 2010, ApJ, 715, 833
Pastorello A. et al., 2004, MNRAS, 347, 74
Pastorello A. et al., 2009, MNRAS, 394, 2266
Pastorello A. et al., 2012, A&A, 537, A141
Patat F., Barbon R., Cappellaro E., Turatto M., 1994, A&A, 282, 731
Persson S. E., Murphy D. C., Krzeminski W., Roth M., Rieke M. J., 1998, AJ, 116, 2475
Planck Collaboration, 2013, A&A, preprint (arXiv:1303.5076)
Poznanski D. et al., 2009, ApJ, 694, 1067
Poznanski D., Ganeshalingam M., Silverman J. M., Filippenko A. V., 2011, MNRAS, 415, L81
Poznanski D., Prochaska J. X., Bloom J. S., 2012, MNRAS, 426, 1465
Pumo M. L., Zampieri L., 2011, ApJ, 741, 41
Pumo M. L., Zampieri L., Turatto M., 2010, MSAIS, 14, 123
Roming P. W. A. et al., 2005, Space Sci. Rev., 120, 95
Roy R. et al., 2011, ApJ, 736, 76
Schlafly E. F., Finkbeiner D. P., 2011, ApJ, 737, 103
Smartt S. J., 2009, ARA&A, 47, 63
Smartt S. J., Eldridge J. J., Crockett R. M., Maund J. R., 2009, MNRAS, 395, 1409
Smith J. A. et al., 2002, AJ, 123, 2121
Stritzinger M. D. et al., 2011, AJ, 142, 156
Takáts K., Vinkó J., 2006, MNRAS, 372, 1735
Takáts K., Vinkó J., 2012, MNRAS, 419, 2783
Tomasella L. et al., 2013, MNRAS, 434, 1636
Tully R. B., 1988, Nearby Galaxies Catalog. Cambridge University Press, Cambridge
Turatto M. et al., 1998, ApJ, 498, L129
Turatto M., Benetti S., Cappellaro E., 2003, in Hillebrandt W., Leibundgut B., eds, From Twilight to Highlight: The Physics of Supernovae: Proceedings of the ESO/MPA/MPE Workshop. Springer-Verlag, Berlin/Heidelberg, p. 200
Utrobin V. P., 2007, A&A, 461, 233
Utrobin V. P., Chugai N. N., 2013, A&A, 555, A145
Utrobin V. P., Chugai N. N., Pastorello A., 2007, A&A, 475, 973
Valenti S. et al., 2011, MNRAS, 416, 3138
Vinkó J. et al., 2004, A&A, 427, 453
Vinkó J. et al., 2012, A&A, 540, A93
Wade R. A., Horne K., 1988, ApJ, 324, 411
Walmswell J. J., Eldridge J. J., 2012, MNRAS, 419, 2054
Zampieri L., 2007, in di Salvo T., Israel G. L., Piersant L., Burderi L., Matt G., Tornambe A., Menna M. T., eds, AIP Conf. Ser. Vol. 924, The Multicolored Landscape of Compact Objects and Their Explosive Origins. Am. Inst. Phys., New York, p. 358
Zampieri L., Pastorello A., Turatto M., Cappellaro E., Benetti S., Altavilla G., Mazzali P., Hamuy M., 2003, MNRAS, 338, 711

Table A1. Summary of the NIR spectroscopic observations of SN 2008in.

Date	JD 240 0000+	Phase[a] (d)	Instrument	Wavelength range μm	Resolution
05/01/2009	54 836.8	11.2	VLT + ISAAC (SWS1-LR)	0.98–2.5	500
10/01/2009	54 841.8	16.2	NTT + SOFI (GB,GR)	0.95–1.64, 1.53–2.52	1000
01/02/2009	54 863.8	38.2	SOAR + OSIRIS (LR)	1.0–2.58	1200
03/02/2009	54 865.9	40.3	VLT + ISAAC (SWS1-LR)	0.98–2.5	500
22/02/2009	54 884.7	59.1	SOAR + OSIRIS (LR)	1.0–2.58	1200
05/03/2009	54 895.7	70.1	VLT + ISAAC (SWS1-LR)	0.98–2.5	500
17/03/2009	54 907.2	81.6	NTT + SOFI (GB,GR)	0.95–1.64, 1.53–2.52	1000

[a]Relative to $t_0 = 245\,4825.6$ JD (Roy et al. 2011).

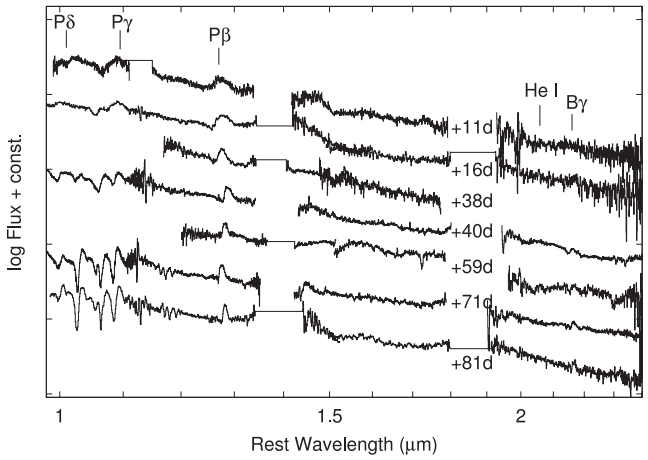

Figure A1. NIR spectra of SN 2008in (see also Fig. 13). The phases are relative to the estimated date of explosion, $t_0 = 245\,4825.6$ JD (Roy et al. 2011).

APPENDIX A: NEAR-INFRARED SPECTRA OF SN 2008IN

In this paper we present seven previously unpublished NIR spectra of SN 2008in taken with VLT/ISAAC, NTT/SOFI and SOAR/OSIRIS telescopes. The summary of the observations can be found in Table A1. The reduction process was the same as for SN 2009N (see Section 3). The NIR spectra of SN 2008in are shown in Fig. A1.

APPENDIX B: PHOTOMETRIC TABLES OF SN 2009N

Table B1. *BVRI* photometry of SN 2009N.

Date	JD−240 0000	*B*	*V*	*R*	*I*	Telescope
27/01/2009	54858.9	16.585 (0.020)	16.274 (0.027)	15.931 (0.020)	15.767 (0.028)	P60
28/01/2009	54859.7	16.474 (0.005)	16.270 (0.004)	15.973 (0.003)	15.815 (0.005)	LT
28/01/2009	54859.8	16.614 (0.030)	16.299 (0.016)	16.019 (0.014)	15.832 (0.014)	PROMPT
29/01/2009	54860.8	16.559 (0.034)	16.331 (0.020)	16.033 (0.015)		PROMPT
29/01/2009	54860.9	16.477 (0.069)	16.247 (0.026)	15.973 (0.028)	15.769 (0.029)	P60
31/01/2009	54862.8	16.590 (0.028)	16.337 (0.009)	15.948 (0.016)	15.751 (0.011)	P60
31/01/2009	54862.8	16.633 (0.023)	16.312 (0.019)	16.006 (0.016)	15.791 (0.015)	PROMPT
01/02/2009	54863.8	16.654 (0.029)	16.290 (0.021)	15.998 (0.017)	15.764 (0.017)	PROMPT
02/02/2009	54864.8	16.694 (0.021)	16.341 (0.014)	15.955 (0.019)	15.664 (0.016)	P60
04/02/2009	54866.8	16.831 (0.025)	16.314 (0.019)	15.978 (0.016)	15.712 (0.016)	PROMPT
06/02/2009	54868.8	16.957 (0.031)	16.347 (0.018)	15.994 (0.016)	15.709 (0.015)	PROMPT
09/02/2009	54871.8		16.369 (0.026)	15.991 (0.015)		PROMPT
12/02/2009	54874.7		16.392 (0.021)	16.004 (0.019)	15.676 (0.018)	PROMPT
15/02/2009	54877.7	17.368 (0.026)	16.393 (0.019)	16.016 (0.015)	15.671 (0.017)	PROMPT
17/02/2009	54879.6			15.937 (0.023)		THO
17/02/2009	54879.7	17.373 (0.034)	16.405 (0.018)	16.005 (0.018)		PROMPT
19/02/2009	54881.6	17.407 (0.012)	16.344 (0.020)	15.889 (0.022)	15.544 (0.033)	CA
19/02/2009	54881.7	17.394 (0.036)	16.392 (0.018)	15.957 (0.016)	15.605 (0.015)	PROMPT
19/02/2009	54881.8	17.343 (0.026)		15.936 (0.011)		P60
19/02/2009	54882.0		16.382 (0.010)		15.564 (0.013)	P60
20/02/2009	54882.6			15.975 (0.023)		CA
21/02/2009	54883.7	17.446 (0.029)	16.374 (0.019)	15.964 (0.015)	15.569 (0.015)	PROMPT
23/02/2009	54885.7	17.432 (0.038)	16.382 (0.017)	15.942 (0.015)	15.541 (0.015)	PROMPT
25/02/2009	54888.5			15.905 (0.022)		THO
26/02/2009	54888.8	17.406 (0.058)	16.352 (0.021)	15.894 (0.031)	15.527 (0.020)	P60
27/02/2009	54889.7	17.547 (0.037)	16.360 (0.019)	15.914 (0.014)	15.506 (0.014)	PROMPT
28/02/2009	54890.7	17.535 (0.032)	16.337 (0.033)	15.949 (0.040)	15.515 (0.011)	P60

Table B1 – *continued*

Date	JD−240 0000	*B*	*V*	*R*	*I*	Telescope
06/03/2009	54896.7	17.761 (0.037)	16.372 (0.018)	15.880 (0.014)	15.455 (0.014)	PROMPT
13/03/2009	54903.7	17.724 (0.058)	16.390 (0.028)	15.892 (0.020)	15.464 (0.026)	PROMPT
15/03/2009	54905.7	17.760 (0.034)	16.413 (0.019)	15.858 (0.015)		PROMPT
17/03/2009	54908.0	17.752 (0.015)		15.857 (0.028)		P60
18/03/2009	54908.6	17.914 (0.039)	16.416 (0.019)	15.859 (0.015)	15.402 (0.014)	PROMPT
19/03/2009	54909.7	17.928 (0.040)	16.414 (0.017)	15.861 (0.014)	15.403 (0.014)	PROMPT
19/03/2009	54910.5			15.823 (0.066)		THO
19/03/2009	54910.5	17.842 (0.010)	16.545 (0.014)	15.853 (0.011)	15.364 (0.016)	CA
20/03/2009	54910.5	17.747 (0.014)	16.470 (0.008)	15.878 (0.014)	15.417 (0.007)	NOT
21/03/2009	54912.5			15.850 (0.018)		THO
22/03/2009	54912.7		16.432 (0.019)	15.857 (0.015)	15.405 (0.014)	PROMPT
24/03/2009	54914.6	17.976 (0.044)	16.434 (0.018)	15.855 (0.014)	15.421 (0.014)	PROMPT
25/03/2009	54915.5			15.854 (0.022)		THO
26/03/2009	54916.6	17.907 (0.051)	16.447 (0.018)	15.880 (0.014)	15.404 (0.014)	PROMPT
26/03/2009	54916.9	17.863 (0.040)	16.505 (0.016)	15.858 (0.007)	15.344 (0.008)	P60
27/03/2009	54917.9	17.850 (0.067)	16.496 (0.030)	15.928 (0.021)	15.403 (0.014)	P60
28/03/2009	54918.6	18.003 (0.055)	16.483 (0.018)	15.873 (0.015)	15.406 (0.014)	PROMPT
28/03/2009	54919.0	17.919 (0.048)	16.527 (0.013)	15.887 (0.011)	15.400 (0.008)	P60
30/03/2009	54921.4	17.956 (0.025)	16.501 (0.006)	15.833 (0.004)	15.467 (0.005)	LT
31/03/2009	54921.0	17.901 (0.030)	16.528 (0.011)	15.873 (0.009)	15.434 (0.008)	P60
01/04/2009	54922.6	17.922 (0.050)	16.503 (0.017)	15.888 (0.014)	15.422 (0.014)	PROMPT
01/04/2009	54923.4	18.045 (0.013)	16.477 (0.007)	15.857 (0.005)	15.460 (0.004)	LT
01/04/2009	54923.5			15.830 (0.024)		THO
05/04/2009	54927.4		16.527 (0.016)		15.452 (0.007)	LT
08/04/2009	54929.6	18.210 (0.069)	16.498 (0.028)	15.947 (0.018)	15.460 (0.018)	PROMPT
11/04/2009	54932.6	18.139 (0.053)	16.598 (0.024)	15.996 (0.016)	15.535 (0.015)	PROMPT
11/04/2009	54933.5	18.210 (0.093)	16.622 (0.017)	16.004 (0.010)	15.570 (0.009)	NOT
11/04/2009	54933.5	18.096 (0.058)	16.686 (0.014)	16.011 (0.012)	15.556 (0.010)	CA
12/04/2009	54933.5	18.133 (0.030)	16.573 (0.013)	15.925 (0.006)	15.557 (0.006)	LT
13/04/2009	54934.7	18.115 (0.022)	16.605 (0.015)	15.999 (0.007)	15.523 (0.020)	P60
13/04/2009	54935.4	18.190 (0.015)	16.628 (0.006)	15.954 (0.009)	15.565 (0.005)	LT
15/04/2009	54937.4			15.989 (0.020)		THO
16/04/2009	54937.6	18.244 (0.030)	16.659 (0.007)	15.968 (0.008)	15.617 (0.008)	LT
18/04/2009	54939.7	18.306 (0.038)	16.708 (0.019)	16.081 (0.015)	15.601 (0.013)	PROMPT
19/04/2009	54941.5	18.327 (0.035)	16.763 (0.009)	16.059 (0.011)	15.672 (0.009)	LT
21/04/2009	54942.6	18.377 (0.056)	16.796 (0.018)	16.133 (0.014)	15.669 (0.015)	PROMPT
23/04/2009	54945.4	18.471 (0.048)	16.886 (0.021)	16.166 (0.008)	15.774 (0.011)	LT
23/04/2009	54945.4			16.191 (0.037)		THO
24/04/2009	54945.6	18.596 (0.052)	16.841 (0.027)			PROMPT
25/04/2009	54946.6			16.280 (0.015)	15.762 (0.014)	PROMPT
25/04/2009	54947.4			16.210 (0.030)		THO
27/04/2009	54948.8	18.545 (0.038)		16.340 (0.005)		P60
28/04/2009	54949.7	18.590 (0.043)	17.090 (0.014)	16.314 (0.009)	15.801 (0.012)	P60
29/04/2009	54950.6	18.712 (0.059)	17.040 (0.022)	16.374 (0.017)	15.906 (0.016)	PROMPT
29/04/2009	54951.4	18.757 (0.021)	17.134 (0.009)	16.387 (0.006)	15.918 (0.006)	LT
30/04/2009	54952.4			16.445 (0.037)		THO
01/05/2009	54952.6	18.726 (0.067)	17.183 (0.022)	16.456 (0.015)	15.995 (0.016)	PROMPT
03/05/2009	54955.4	19.114 (0.025)	17.483 (0.010)	16.701 (0.008)	16.215 (0.007)	LT
04/05/2009	54955.6		17.469 (0.032)	16.730 (0.018)	16.185 (0.019)	PROMPT
07/05/2009	54958.5	19.075 (0.276)	18.343 (0.155)	17.261 (0.068)	16.864 (0.066)	PROMPT
08/05/2009	54960.4	20.201 (0.048)	18.504 (0.018)	17.690 (0.020)	17.069 (0.008)	NOT
09/05/2009	54960.6		18.388 (0.082)	17.558 (0.038)	16.967 (0.035)	PROMPT
10/05/2009	54961.7	19.474 (0.143)		17.580 (0.038)	16.993 (0.035)	PROMPT
11/05/2009	54962.6			17.575 (0.033)	17.095 (0.029)	PROMPT
11/05/2009	54963.4	20.438 (0.058)	18.808 (0.022)	17.693 (0.014)	17.158 (0.010)	LT
12/05/2009	54963.6	20.126 (0.193)	18.575 (0.076)	17.633 (0.031)	17.108 (0.029)	PROMPT
12/05/2009	54963.7	20.347 (0.451)	18.739 (0.099)	17.677 (0.060)	17.123 (0.015)	P60
13/05/2009	54964.6	20.172 (0.155)	18.641 (0.065)	17.643 (0.031)	17.142 (0.022)	PROMPT
13/05/2009	54964.7	20.374 (0.299)	18.774 (0.083)	17.704 (0.041)	17.060 (0.010)	P60
16/05/2009	54968.4	20.509 (0.087)	18.796 (0.054)	17.785 (0.017)	17.222 (0.018)	LT
20/05/2009	54971.6		18.890 (0.130)	17.707 (0.039)	17.184 (0.050)	PROMPT
22/05/2009	54973.6		18.665 (0.053)	17.735 (0.026)	17.172 (0.021)	PROMPT
22/05/2009	54974.5	20.576 (0.304)	18.941 (0.032)	17.792 (0.018)	17.236 (0.023)	LT
24/05/2009	54975.7	20.395 (0.190)	18.919 (0.068)	17.867 (0.028)	17.277 (0.013)	P60

Table B1 – *continued*

Date	JD−2400000	*B*	*V*	*R*	*I*	Telescope
25/05/2009	54977.4	20.499 (0.188)	18.941 (0.049)	17.830 (0.023)	17.304 (0.017)	LT
27/05/2009	54978.7		18.979 (0.025)	17.882 (0.017)	17.248 (0.035)	P60
30/05/2009	54982.4	20.527 (0.073)	18.975 (0.041)	17.860 (0.012)	17.375 (0.018)	LT
05/06/2009	54987.7		18.925 (0.125)	17.970 (0.038)	17.350 (0.056)	P60
12/07/2009	54994.6		18.864 (0.067)	17.884 (0.022)	17.359 (0.021)	PROMPT
27/06/2009	55009.7		19.096 (0.033)	18.076 (0.015)	17.505 (0.045)	P60
02/07/2009	55014.7		19.120 (0.091)	18.127 (0.038)	17.621 (0.023)	P60
18/07/2009	55031.5		19.344 (0.040)	18.306 (0.026)	17.713 (0.070)	CTIO
23/07/2009	55036.5		19.364 (0.038)	18.432 (0.020)	17.758 (0.018)	CTIO
29/07/2009	55042.5		19.423 (0.032)	18.451 (0.017)	17.796 (0.023)	CTIO
23/01/2010	55219.8		21.035 (0.075)	20.419 (0.068)	19.890 (0.070)	NTT
20/02/2010	55247.7		21.160 (0.049)	20.571 (0.044)	20.017 (0.122)	NTT
05/03/2010	55260.8		21.256 (0.056)	20.670 (0.052)	20.142 (0.044)	NTT

Telescope: P60 - Palomar 1.5-m telescope; LT - 2.0-m Liverpool Telescope + RatCAM; PROMPT - Panchromatic Robotic Optical Monitoring and Polarimetry Telescopes; THO - 14 arcsec Telescope at Taurus Hill Observatory + ST-8XME; CA - 2.2m Calar Alto + CAFOS; NOT - 2.6-m Nordic Optical Telescope + ALFOSC; CTIO - CTIO 1.3 m SMARTS telescope + ANDICAM; NTT - 3.6-m New Technology Telescope + EFOSC2.

Table B2. $g'r'i'z'$ photometry of SN 2009N taken with the *PROMPT* telescopes.

Date	JD−240 0000	g'	r'	i'	z'
31/01/2009	54862.8	16.450 (0.015)	16.143 (0.034)	16.102 (0.017)	16.067 (0.024)
01/02/2009	54863.8	16.501 (0.017)	16.134 (0.035)	16.050 (0.017)	15.976 (0.021)
04/02/2009	54866.8	16.533 (0.018)	16.132 (0.035)	16.053 (0.019)	15.931 (0.019)
06/02/2009	54868.8	16.627 (0.018)	16.138 (0.034)	16.050 (0.017)	15.948 (0.020)
08/02/2009	54870.8	16.672 (0.017)	16.166 (0.035)	16.039 (0.018)	
12/02/2009	54874.8		16.168 (0.035)	16.026 (0.020)	15.894 (0.026)
11/02/2009	54874.8		16.168 (0.035)	16.026 (0.020)	15.894 (0.026)
15/02/2009	54877.8	16.780 (0.015)	16.171 (0.034)	16.017 (0.017)	15.824 (0.021)
17/02/2009	54879.7	16.824 (0.016)	16.151 (0.035)		
19/02/2009	54881.7	16.808 (0.017)	16.148 (0.034)	15.955 (0.017)	15.834 (0.022)
21/02/2009	54883.7	16.835 (0.018)	16.134 (0.034)	15.932 (0.016)	15.783 (0.020)
23/02/2009	54885.7	16.830 (0.018)	16.132 (0.034)	15.904 (0.017)	15.740 (0.020)
27/02/2009	54889.7	16.847 (0.018)	16.099 (0.034)	15.861 (0.016)	15.706 (0.019)
06/03/2009	54896.7	16.901 (0.016)	16.086 (0.034)	15.814 (0.015)	15.664 (0.018)
13/03/2009	54903.7	16.949 (0.022)	16.056 (0.039)	15.730 (0.024)	15.597 (0.042)
15/03/2009	54905.7		16.061 (0.034)	15.763 (0.016)	15.615 (0.021)
18/03/2009	54908.7	17.016 (0.015)	16.059 (0.034)	15.755 (0.016)	15.586 (0.022)
19/03/2009	54909.7	17.017 (0.017)	16.059 (0.034)	15.773 (0.015)	15.611 (0.018)
22/03/2009	54912.6		16.068 (0.035)	15.760 (0.016)	15.613 (0.020)
24/03/2009	54914.6	17.079 (0.017)	16.074 (0.034)	15.778 (0.016)	15.634 (0.019)
26/03/2009	54916.6	17.101 (0.019)	16.070 (0.035)	15.774 (0.016)	15.615 (0.020)
28/03/2009	54918.7	17.104 (0.019)	16.084 (0.034)	15.787 (0.016)	15.606 (0.021)
01/04/2009	54922.6	17.115 (0.020)	16.075 (0.034)	15.780 (0.017)	15.645 (0.020)
08/04/2009	54929.6	17.192 (0.027)	16.176 (0.037)	15.871 (0.022)	15.743 (0.026)
11/04/2009	54932.6	17.242 (0.023)	16.206 (0.036)	15.848 (0.017)	15.772 (0.022)
18/04/2009	54939.7	17.376 (0.018)	16.259 (0.034)	15.946 (0.016)	15.800 (0.019)
21/04/2009	54942.6	17.412 (0.023)	16.340 (0.035)	16.019 (0.016)	15.851 (0.021)
24/04/2009	54945.6	17.561 (0.020)	16.413 (0.040)	16.095 (0.023)	
29/04/2009	54950.6	17.686 (0.040)	16.596 (0.034)	16.251 (0.019)	16.076 (0.021)
01/05/2009	54952.6	17.866 (0.023)	16.649 (0.034)	16.334 (0.018)	16.165 (0.023)
04/05/2009	54955.6	18.203 (0.030)	16.917 (0.036)	16.605 (0.021)	16.432 (0.029)
07/05/2009	54958.6	18.540 (0.204)	17.662 (0.090)		
09/05/2009	54960.6		17.752 (0.050)	17.395 (0.035)	17.106 (0.048)
10/05/2009	54961.6	19.008 (0.061)	17.823 (0.046)	17.463 (0.029)	17.193 (0.050)
11/05/2009	54962.6		17.900 (0.043)		17.097 (0.051)
12/05/2009	54963.5	19.049 (0.043)	17.926 (0.041)	17.473 (0.029)	17.295 (0.047)
23/05/2009	54974.6	19.387 (0.066)	17.982 (0.041)	17.634 (0.026)	17.271 (0.042)
13/05/2009	54995.5		18.124 (0.040)	17.900 (0.025)	17.500 (0.035)

Table B3. *BVRI* magnitudes of the local sequence stars.

Star	α_{J2000}	δ_{J2000}	*B*	*V*	*R*	*I*
1	12:31:09.006	−08:04:35.29	20.612 (0.238)	19.225 (0.090)	18.659 (0.031)	17.979 (0.043)
2	12:31:10.321	−08:03:56.69	19.115 (0.076)	18.158 (0.066)	17.607 (0.040)	17.026 (0.043)
3	12:31:15.903	−08:02:14.07	17.276 (0.101)	16.665 (0.051)	16.316 (0.038)	15.893 (0.035)
4	12:31:15.307	−08:01:58.17	15.819 (0.088)	15.118 (0.045)	14.734 (0.031)	14.316 (0.036)
5	12:31:08.100	−08:02:01.29	17.016 (0.074)	16.252 (0.051)	15.848 (0.035)	15.411 (0.044)
6	12:31:03.358	−08:02:13.81	13.821 (0.078)	12.920 (0.050)	12.457 (0.029)	11.969 (0.040)
7	12:30:57.996	−08:01:32.58	16.384 (0.064)	15.624 (0.049)	15.215 (0.026)	14.756 (0.036)
8	12:30:57.482	−08:05:28.19	18.745 (0.163)	17.043 (0.051)	16.070 (0.030)	14.836 (0.053)
9	12:31:01.452	−08:06:14.02	15.125 (0.061)	14.335 (0.049)	13.941 (0.035)	13.545 (0.028)
10	12:31:07.750	−08:06:39.12	17.154 (0.053)	16.370 (0.048)	15.959 (0.036)	15.514 (0.032)
11	12:31:19.407	−08:07:03.51	18.151 (0.983)	16.936 (0.078)	16.721 (0.038)	16.380 (0.037)
12	12:31:22.057	−08:06:19.63	18.379 (0.090)	16.699 (0.045)	15.753 (0.025)	14.481 (0.049)
13	12:31:25.355	−08:06:37.04	20.780 (0.010)	15.838 (0.056)	15.508 (0.042)	15.086 (0.034)
14	12:31:24.593	−08:03:59.05	20.780 (0.010)	13.829 (0.043)	13.537 (0.032)	13.183 (0.032)
15	12:31:14.787	−08:03:38.06	13.298 (0.073)	12.607 (0.049)	12.250 (0.038)	11.884 (0.029)
16	12:31:27.718	−08:02:34.53	20.780 (0.010)	12.659 (0.489)	11.671 (0.083)	11.117 (0.025)
17	12:31:28.057	−08:01:05.10	20.780 (0.010)	18.141 (2.299)	19.332 (6.133)	15.229 (0.013)
18	12:31:21.260	−08:00:22.14	17.736 (0.122)	17.140 (0.060)	16.809 (0.031)	16.444 (0.045)
19	12:31:21.166	−08:00:11.70	18.639 (0.096)	17.190 (0.056)	16.290 (0.035)	15.166 (0.011)
20	12:31:17.638	−07:59:52.25	16.493 (0.094)	15.954 (0.042)	15.641 (0.027)	15.269 (0.032)
21	12:31:12.089	−08:00:13.41	15.418 (0.107)	14.828 (0.047)	14.509 (0.028)	14.143 (0.036)
22	12:31:06.949	−07:59:24.83	17.077 (0.084)	16.519 (0.045)	16.213 (0.034)	15.860 (0.030)
23	12:31:05.295	−07:59:05.75	17.953 (0.139)	16.986 (0.039)	16.440 (0.019)	15.882 (0.029)
24	12:31:05.463	−07:58:54.88	18.738 (0.030)	17.192 (0.054)	16.344 (0.016)	15.497 (0.045)

Table B4. $g'r'i'z'$ magnitudes of the local sequence stars.

Star	α_{J2000}	δ_{J2000}	g'	r'	i'	z'
1	12:31:09.006	−08:04:35.29				
2	12:31:10.321	−08:03:56.69	18.643 (0.010)	17.836 (0.056)	17.527 (0.114)	17.329 (0.064)
3	12:31:15.903	−08:02:14.07	16.916 (0.046)	16.491 (0.054)	16.332 (0.066)	16.257 (0.047)
4	12:31:15.307	−08:01:58.17	15.431 (0.035)	14.905 (0.056)	15.565 (2.424)	14.687 (0.046)
5	12:31:08.100	−08:02:01.29	16.593 (0.025)	16.042 (0.041)	15.858 (0.050)	15.783 (0.048)
6	12:31:03.358	−08:02:13.81	13.335 (0.027)	12.666 (0.039)	12.423 (0.045)	12.295 (0.027)
7	12:30:57.996	−08:01:32.58	15.960 (0.024)	15.405 (0.035)	15.200 (0.043)	15.101 (0.036)
8	12:30:57.482	−08:05:28.19	17.889 (0.088)	16.399 (0.042)	15.463 (0.053)	14.992 (0.039)
9	12:31:01.452	−08:06:14.02	14.700 (0.035)	14.132 (0.031)	13.985 (0.038)	13.926 (0.037)
10	12:31:07.750	−08:06:39.12	16.723 (0.049)	16.141 (0.046)	15.994 (0.068)	15.906 (0.061)
11	12:31:19.407	−08:07:03.51				
12	12:31:22.057	−08:06:19.63	17.465 (0.109)	16.097 (0.043)	15.128 (0.054)	14.650 (0.051)
13	12:31:25.355	−08:06:37.04		15.677 (0.049)	15.600 (0.115)	15.505 (0.052)
14	12:31:24.593	−08:03:59.05	19.876 (0.010)	13.723 (0.063)	13.617 (0.053)	13.590 (0.032)
15	12:31:14.787	−08:03:38.06	12.926 (0.026)	12.426 (0.049)	12.314 (0.045)	12.270 (0.029)
16	12:31:27.718	−08:02:34.53	19.954 (0.010)	11.940 (0.026)	11.645 (0.059)	11.456 (0.033)
17	12:31:28.057	−08:01:05.10		16.027 (0.059)	15.739 (0.050)	
18	12:31:21.260	−08:00:22.14	17.396 (0.053)	16.982 (0.025)	16.894 (0.058)	16.825 (0.057)
19	12:31:21.166	−08:00:11.70	17.893 (0.073)	16.600 (0.039)	15.808 (0.069)	15.358 (0.028)
20	12:31:17.638	−07:59:52.25	16.181 (0.047)	15.793 (0.053)	15.710 (0.055)	15.673 (0.058)
21	12:31:12.089	−08:00:13.41	15.088 (0.027)	14.665 (0.066)	14.579 (0.049)	14.534 (0.039)
22	12:31:06.949	−07:59:24.83	16.754 (0.027)	16.378 (0.036)	16.280 (0.047)	16.246 (0.050)
23	12:31:05.295	−07:59:05.75	17.425 (0.057)	16.651 (0.042)	16.375 (0.074)	16.202 (0.065)
24	12:31:05.463	−07:58:54.88	17.900 (0.125)	16.612 (0.038)	16.050 (0.055)	15.715 (0.058)

Table B5. *YJH* magnitudes of local sequence stars.

Star	α_{J2000}	δ_{J2000}	*Y*	*J*	*H*
A	12:33:29.431	−08:19:01.37		13.687 (0.029)	13.223 (0.022)
B	12:33:46.507	−08:14:55.17		10.875 (0.041)	
C	12:33:38.513	−08:18:46.20		11.330 (0.029)	10.834 (0.039)
D	12:33:49.944	−08:20:10.46	11.634 (0.023)	11.467 (0.029)	11.100 (0.019)
E	12:33:59.758	−08:20:31.31	13.017 (0.016)	12.833 (0.013)	12.534 (0.015)
F	12:33:36.620	−08:22:46.41		13.056 (0.036)	12.710 (0.017)
G	12:33:57.231	−08:22:51.81	13.825 (0.023)	13.395 (0.018)	12.843 (0.017)
H	12:33:47.233	−08:16:46.01	13.909 (0.023)	13.707 (0.017)	13.301 (0.016)
I	12:33:50.461	−08:18:30.49	14.036 (0.016)	13.794 (0.013)	13.384 (0.012)
J	12:33:32.643	−08:22:00.73		13.751 (0.029)	13.169 (0.022)
K	12:33:51.115	−08:24:45.67	14.422 (0.023)	14.238 (0.019)	13.932 (0.020)
L	12:33:33.144	−08:18:05.07		14.152 (0.030)	13.687 (0.022)
M	12:33:40.223	−08:24:53.96	14.623 (0.023)	14.226 (0.019)	13.645 (0.019)
N	12:33:56.318	−08:16:44.15	14.556 (0.023)	14.139 (0.017)	13.501 (0.016)
O	12:34:00.534	−08:23:09.27	14.911 (0.023)	14.679 (0.019)	14.340 (0.023)
P	12:33:52.784	−08:16:24.71	15.066 (0.023)	14.861 (0.018)	14.465 (0.018)
Q	12:33:42.916	−08:23:11.40	15.272 (0.024)	14.982 (0.019)	14.574 (0.021)
R	12:33:35.132	−08:14:41.83		14.891 (0.039)	14.271 (0.033)
S	12:33:50.302	−08:14:51.64	15.319 (0.024)	15.014 (0.037)	14.487 (0.020)
T	12:33:30.343	−08:19:45.39		15.306 (0.032)	14.821 (0.028)
U	12:33:56.389	−08:14:46.54	15.557 (0.026)	15.325 (0.021)	14.976 (0.032)
V	12:33:51.064	−08:18:46.28	15.628 (0.018)	15.378 (0.014)	14.970 (0.017)

Table B6. NIR photometry of SN 2009N.

Date	JD−240 0000	*Y*	*J*	*H*
26/01/2009	54857.8	15.738 (0.017)	15.604 (0.014)	15.369 (0.023)
29/01/2009	54860.8	15.709 (0.014)	15.518 (0.018)	15.278 (0.022)
24/02/2009	54886.8	15.306 (0.018)	15.070 (0.017)	14.751 (0.015)
25/02/2009	54887.8	15.291 (0.017)	15.047 (0.017)	14.747 (0.017)
28/02/2009	54890.8	15.268 (0.015)	15.007 (0.014)	14.739 (0.017)
05/03/2009	54895.9	15.206 (0.014)	14.971 (0.018)	14.649 (0.019)
11/03/2009	54901.7	15.180 (0.014)	14.941 (0.017)	14.620 (0.015)
22/03/2009	54912.9	15.197 (0.014)	14.927 (0.018)	14.590 (0.016)
29/03/2009	54919.8	15.213 (0.023)	14.919 (0.018)	14.600 (0.021)
24/04/2009	54945.7	15.558 (0.014)	15.298 (0.015)	14.910 (0.017)
19/03/2010	55274.7	20.538 (0.378)	20.171 (0.239)	19.110 (0.390)
19/03/2010	55274.8	20.602 (0.335)	20.540 (0.487)	

Table B7. *Swift* photometry of SN 2009N.

Date	JD−240 0000	*uvw*2	*uvm*2	*uvw*1	*u*	*b*	*v*
27/01/2009	54858.8	16.885 (0.068)	16.711 (0.062)	16.200 (0.053)	15.599 (0.047)	16.541 (0.043)	16.351 (0.049)
29/01/2009	54861.0	17.618 (0.099)	17.615 (0.137)	16.848 (0.082)	15.873 (0.059)	16.657 (0.057)	16.423 (0.077)
01/02/2009	54863.8	18.404 (0.089)	18.477 (0.121)	17.664 (0.072)	16.254 (0.049)	16.693 (0.043)	16.298 (0.048)
04/02/2009	54867.2	18.740 (0.100)	18.792 (0.130)	18.047 (0.082)	16.892 (0.055)	16.820 (0.044)	16.394 (0.048)
16/03/2009	54907.3	19.035 (0.107)	18.996 (0.146)	19.069 (0.134)	18.781 (0.113)	17.765 (0.051)	16.474 (0.046)

This paper has been typeset from a TEX/LATEX file prepared by the author.